

Article

Reliability of Gridded Precipitation Products in the Yellow River Basin, China

Yanfen Yang ¹, Jing Wu ², Lei Bai ³ and Bing Wang ^{1,*}

¹ State Key Laboratory of Soil Erosion and Dryland Farming on the Loess Plateau, Institute of Soil and Water Conservation, Northwest A&F University, Yangling 712100, China; yfyang@ms.iswc.ac.cn

² Lanzhou Central Meteorological Observatory, Lanzhou 730020, China; Wujing10@mailsucas.ac.cn

³ School of Navigation, Wuhan University of Technology, Wuhan 430070, China; bailei09@mailsucas.ac.cn

* Correspondence: bwang@ms.iswc.ac.cn; Tel.: +86-1582-991-2700

Received: 25 December 2019; Accepted: 20 January 2020; Published: 23 January 2020



Abstract: Gridded precipitation products are the potential alternatives in hydrological studies, and the evaluation of their accuracy and potential use is very important for reliable simulations. The objective of this study was to investigate the applicability of gridded precipitation products in the Yellow River Basin of China. Five gridded precipitation products, i.e., Multi-Source Weighted-Ensemble Precipitation (MSWEP), CPC Morphing Technique (CMORPH), Global Satellite Mapping of Precipitation (GSMaP), Tropical Rainfall Measuring Mission (TRMM) Multi-Satellite Precipitation Analysis 3B42, and Precipitation Estimation from Remotely Sensed Information using Artificial Neural Networks (PERSIANN), were evaluated against observations made during 2001–2014 at daily, monthly, and annual scales. The results showed that MSWEP had a higher correlation and lower percent bias and root mean square error, while CMORPH and GSMaP made overestimations compared to the observations. All the datasets underestimated the frequency of dry days, and overestimated the frequency and the intensity of wet days (0–5 mm/day). MSWEP and TRMM showed consistent interannual variations and spatial patterns while CMORPH and GSMaP had larger discrepancies with the observations. At the sub-basin scale, all the datasets performed poorly in the Beiluo River and Qingjian River, whereas they were applicable in other sub-basins. Based on its superior performance, MSWEP was identified as more suitable for hydrological applications.

Keywords: precipitation datasets; evaluation; spatial scale; temporal scale; climate; Yellow River Basin

1. Introduction

Precipitation is the main link in the hydrological cycle and one of the most important meteorological input elements of hydrological models. Accurate precipitation input is the basic condition for obtaining reliable land surface hydrological simulations [1]. Choosing precipitation data is more important than choosing hydrological models [2]. The use of ground rainfall observation stations is the most direct way to measure precipitation. However, rain gauge density in complex terrain is low and unevenly distributed, thereby resulting in scarce or even a lack of observed precipitation, which cannot meet the needs of hydrological simulations. Remote sensing products based on microwave (MW) and infrared (IR) measurements have become a potential and valuable data source owing to their wide coverage and high spatiotemporal resolution. Affected by sampling error, algorithm uncertainty [3–6], the number of stations [7,8], and topographical factors [9,10], gridded precipitation data have errors when comparing to gauge observations, and rigorous quality assessment is required before use.

In recent years, precipitation products have been evaluated at multi-regional, multi-temporal, and multi-spatial scales; the results showed that there are large differences among precipitation products. Beck and Vergopolan [11] evaluated 22 precipitation products at the global scale. Among the

uncorrected datasets, the satellite and reanalysis-based Multi-Source Weighted-Ensemble Precipitation (MSWEP)-ng (the full name of the abbreviation was listed in Table 1, the same below) showed the greatest correlation with the observations, followed by the reanalysis data (ERA-Interim, JRA-55, and NCEP CFSR), satellite-reanalysis data (CHIRP), passive MW-based data (CPC Morphing Technique (CMORPH), Global Satellite Mapping of Precipitation (GSMaP_MVK), and Tropical Rainfall Measuring Mission (TRMM) 3B42RT), and products based on IR imagery (GridSat, Precipitation Estimation from Remotely Sensed Information using Artificial Neural Networks (PERSIANN), and PERSIANN-CCS). Among the corrected datasets, the products that directly merge daily gauge observations perform best (CPC Unified and MSWEP), followed by those that incorporate temporally coarser gauge data (CHIRPS, GPCP-1DD, TRMM 3B42, and WFDEI-CRU) and products that indirectly incorporate gauge data through other multi-source datasets (PERSIANN-CDR). In China, the spatial distribution of daily mean precipitation of CMORPH and TRMM 3B42 shows good similarity with the ground station data, and both can describe the diurnal variation in summer precipitation in most regions of China [12]. CMORPH outperforms GSMaP_MVK and PERSIANN [13], and IMERG performs better than TRMM 3B42, CMORPH_CRT, and PERSIANN_CDR [14]. The corrected GSMaP_Gauge is superior to GSMaP_NRT and GSMaP_MVK [15]. In humid regions of China, TRMM 3B42 shows the lowest error and deviation and the highest correlation coefficient (CC) at a monthly scale, but its accuracy is lower at a daily scale compared with that of PERSIANN_CDR and NCEP-CFSR [16]. In the Qinghai-Tibet Plateau, IMERG is superior to TRMM 3B42V7 at multiple time scales, but with discrepancies in the timing of the greatest precipitation intensity and overestimation of the maximum rainfall intensity [17]. The error and deviation of TRMM 3B42 are lower than those of PERSIANN and CMORPH [18,19]. In addition, TRMM 3B42 and CMORPH_BLD outperform CMORPH and TRMM 3B42RT in the Huifa River Basin [20]. IMERG is superior to TRMM 3B42 in detecting precipitation events and precipitation in the Huai River Basin [21]. Compared with PERSIANN_CDR, CHIRPS shows a lower bias (PBIAS) and error, and can describe the spatial pattern of precipitation at a monthly and annual scale more accurately in Xinjiang Province [22].

Table 1. Full name of the abbreviation in the text.

Abbreviation	Full Name
CFSR	Climate Forecast System Reanalysis
CHIRP	Climate Hazards group Infrared Precipitation
CHIRPS	Climate Hazards group Infrared Precipitation with Stations
CMORPH	Climate Prediction Center MORPHing technique
CMORPH_BLD	CMORPH satellite-gauge blended product
CMORPH_CRT	CMORPH bias corrected
CPC	Climate Prediction Center
ERA-Interim	European Centre for Medium-range Weather Forecasts ReAnalysis Interim
GPCP	Global Precipitation Climatology Project
GPCP-1DD	GPCP 1-Degree Daily
GridSat	P derived from the Gridded Satellite
GSMaP_MVK	Global Satellite Mapping of Precipitation (GSMaP) Moving Vector with Kalman (MVK)
GSMaP_NRT	GSMaP Near Real Time
IMERG	Integrated Multi-satellite Retrievals for Global Precipitation Measurement
JRA-55	Japanese 55-year ReAnalysis
MSWEP	Multi-Source Weighted-Ensemble Precipitation
NCEP	National Centers for Environmental Prediction
PERSIANN	Precipitation Estimation from Remotely Sensed Information using Artificial Neural Networks
PERSIANN-CCS	PERSIANN Cloud Classification System

Table 1. Cont.

Abbreviation	Full Name
PERSIANN-CDR	PERSIANN Climate Data Record
TMPA	TRMM Multi-satellite Precipitation Analysis
TRMM	Tropical Rainfall Measuring Mission
WFDEI-CRU	WATCH Forcing Data ERA-Interim Climatic Research Unit

The same type of precipitation product shows different performance in different regions and at different temporal scales. MSWEP generally overestimates the precipitation in China but underestimates it in North China. MSWEP overestimates light precipitation but underestimates the heavy precipitation events. It shows the highest accuracy at a monthly scale and the lowest accuracy at a daily scale. There is a significant difference in the annual trend of precipitation between MSWEP and the observations [23]. PERSIANN_CDR can capture the spatiotemporal characteristics of extreme precipitation events at a daily scale in the southeast monsoon region of China [24]. It is also a reliable alternative dataset in the Qinghai-Tibet Plateau, upper Yellow River (UYR) [25], and Xiang River Basin [16]. CMORPH shows a large error in the southeast and poor time correlation of seasonal precipitation in the west and northwest of China [14]. IMERG and TRMM 3B42V7 mostly show high correlation and low relative error in the eastern river basins while showing low correlation and high relative error in the western region of China [26]. The performance of precipitation products also varies seasonally. In China, satellite precipitation and site-corrected products have poor ability to detect precipitation events in winter [12]. IMERG has a stronger ability for light and solid precipitation, and its accuracy for winter precipitation is significantly higher than that of TRMM 3B42, but its accuracy in detecting heavy precipitation needs to be strengthened [26].

The Yellow River Basin in China is characterized by a wide area, complex topography and landforms, diverse climate types, and vegetation coverage. The rain gauges here are unevenly distributed with low density, and have poorly representative and discontinuous data sequences, which cannot meet the needs of hydrological simulations. Sometimes, there is only one to two or even no stations in a target research basin, which often leads to great uncertainty in the input precipitation and poor prediction of the rainfall-runoff model [27]. Gridded precipitation datasets have the potential to improve the quality of precipitation and runoff prediction results. In the Yellow River Basin, it had been reported that there is a good linear relationship between IMERG, TRMM 3B42V7, and ground-based rain gauge data, but the annual precipitation is overestimated by 2.46% and 2.19%, respectively. The CC is relatively high in the southern part of the basin, while the correlation is relatively low in the Ordos Plateau and its north [28]. Seasonally, IMERG and TRMM 3B42 show higher reproducibility in spring and autumn than in winter and summer. The precipitation is underestimated in July and August but is overestimated to different degrees in other months. Among them, the relative error is the largest in December, and the absolute deviation is the largest in September [28].

In summary, the accuracy of precipitation products varies with regions, seasons, and spatiotemporal scales. However, studies in the Yellow River Basin are generally conducted at a large spatial scale, thereby masking the error distribution of small-scale watersheds. In addition, it was common that only one or two products were evaluated, which may result in lacking comprehensive cognition of other kinds of products. The objective of this study was to evaluate of the applicability of multiple precipitation datasets at multiple spatiotemporal scales in the Yellow River Basin in order to provide a reliable source of precipitation data for hydrological simulation and water resources management.

2. Study Area and Methods

2.1. Study Area

The Yellow River Basin, which is located between 96–119°E and 32–42°N, has a drainage area of 7,950,000 km² [29]. The basin traverses the Qinghai-Tibet Plateau, Inner Mongolia Plateau,

Loess Plateau, and Huanghuaihai Plain from the west to the east [30]. The Yellow River Basin belongs to the continental monsoon climate and can be roughly divided into arid, semi-arid, semi-humid, and humid climates [29]. The west is arid, while the east is humid. It is dry in winter with drought in spring, and is rainy in summer and autumn [31]. Affected by the topography and atmospheric circulation, the precipitation is unevenly distributed across the seasons, with large interannual and regional variations. Nine provinces are involved in the Yellow River Basin: Qinghai, Sichuan, Gansu, Ningxia, Inner Mongolia, Shaanxi, Shanxi, Henan and Shandong. The drainage area in Shandong Province is long and narrow, and will not be discussed in this study. The basin was divided into seven water systems to facilitate the evaluation at different regional and spatial scales, including the UYR, Gansu–Ningxia water system (GN), Inner Mongolia water system (IM), Northern Shaanxi water system (NSH), Wei River Basin (WR), Fen River Basin (FR), and Western Henan water system (WH). Furthermore, the basin was divided into 24 sub-basins, including the Yellow River source region, Wuding River, and Jing River. The geographical location, elevation, rain gauge distribution, water system division, and sub-basin division of the Yellow River Basin are shown in Figure 1.

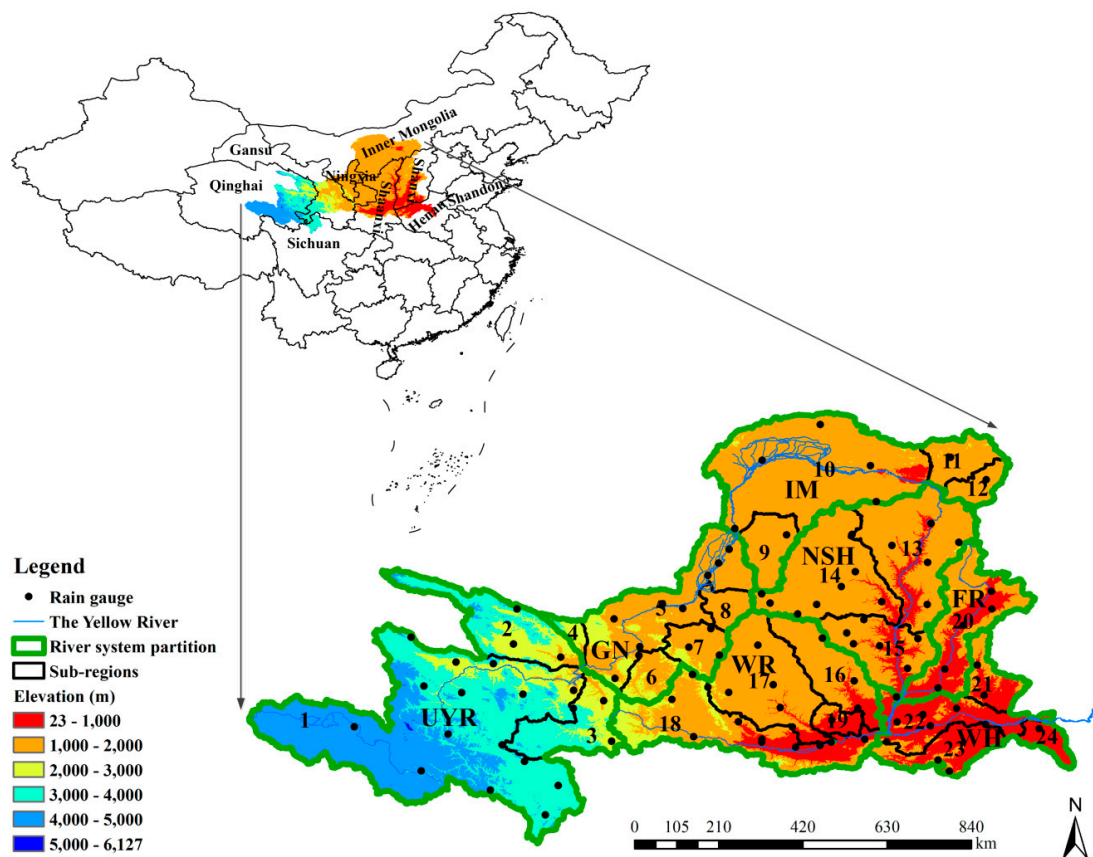


Figure 1. Geographical location, elevation, rain gauge distribution, water system partition and sub-basins of the Yellow River basin. UYR, GN, IM, NSH, WR, FR, and WH are the upper Yellow River, Gansu–Ningxia water system, Inner Mongolia water system, Northern Shaanxi water system, Wei River Basin, Fen River Basin, Western Henan water system, respectively. The No and the name of the sub-basins: 1, Yellow River Source. 2, Huang River. 3, Tao River. 4, Zhuanglang River. 5, Tributary 1 in upper Yellow River. 6, Zuli River. 7, Qingshui River. 8, Kushui River. 9, Dusitu River. 10, Tributary 2 in upper Yellow River. 11, Dahei River. 12, Hun River. 13, Tuwei River, Kuye River, etc. 14, Wuding River. 15, Qingjian River and Yanshui River. 16, Beiluo River. 17, Jing River. 18, Wei River. 19, Shichuan River. 20, Fen River. 21, Qin River. 22, Tributary in middle Yellow River. 23, Yiluo River. 24, Ying River.

2.2. Datasets

The gauge observed daily precipitation (OBS) was used to conduct the point to point evaluation. The gridded dataset CN05.1 interpolated from OBS was used as a reference to evaluate the spatial patterns of the precipitation products. Both OBS and CN05.1 were obtained from the National Meteorological Information Center of China. CN05.1 was interpolated based on the daily precipitation of 2416 rain gauges around China. The spatial resolution was $0.25^\circ \times 0.25^\circ$ and the temporal resolution was daily [32]. The interpolation of CN05.1 was realized by the “anomaly approach”. The climatology was first interpolated by thin-plate smoothing splines and then a gridded daily anomaly derived from angular distance weighting method was added to climatology to obtain the final dataset. New and Lister [33] compared several kinds of interpolation methods and indicated that these two methods performed better. Gridded precipitation such as CN05, EA05 and APHRO were all interpolated by using these methods [34–36]. The climatology was first interpolated due to climatic factors, especially precipitation, have great discontinuity in spatial distribution. The climatology is relatively continuous; interpolating it first is beneficial to reduce errors caused by discontinuity. Specifically, thin-plate smoothing splines is used to interpolate climatology by a software named ANUSPLIN. ANUSPLIN was a interpolation package that was widely used to produce climatic elements with high resolution in geography and ecology [37]. CN05.1 was interpolated using ANUSPLIN, taking longitude and latitude as independent variable, and taking elevation as covariable. Then, the anomaly was derived from an angular distance weighting method. The grid value was obtained on the consideration of the weight of angle and distance between the gauge station and the grid.

Five precipitation products were evaluated, including CMORPH_bleneded, PERSIANN_CDR, GSMaP_MVK, MSWEP V1.1 and TRMM 3B42 V7. Basic information about the products is shown in Table 2. The coarsest temporal and spatial resolutions were daily and 0.25° , and the highest resolutions were 1 h and 0.1° , respectively. To facilitate the point to point evaluation, all the products were downscaled to the spatial location of rain gauge using the bilinear interpolation method. In this method, four nearest grid values are used for calculating the value of a particular point. The weights are derived from the spatial locations in a two-dimensional space. The closer the grid is to the point, the more influence (weight) it will have. The algorithm obtains the pixel value by taking a weighted sum of the pixel values of the four nearest neighbors surrounding the calculated location [38,39]. The raw CMORPH, which was retrieved from MW and IR signals, is a pure satellite precipitation product with a spatial resolution of 8 km and temporal resolution of 30 min [40]. CMORPH_bleneded is a dataset incorporating raw CMORPH and 30,000 automatic meteorological stations around China, and the spatial and temporal resolutions were 0.1° and 1 h, respectively [41].

Table 2. Brief introduction of precipitation datasets in this study.

Dataset		Time Span	Temporal Resolution	Spatial Resolution	Data Source
Full Name	Abbreviation				
CMORPH_bleneded	CMORPH	1998–present	Hourly	0.10°	IR, SSM/I, TRMM, AMSU-B, AMSR-E, Automatic weather station in China
PERSIANN_CDR	PERSIANN	1983–2017	Daily	0.25°	IR, TRMM 2A12, NCEP IV, GPCP
TMPA 3B42 V7	TRMM	1998–2016	3 hourly	0.25°	IR, SSMIS, TMI, AMSU-B, MHS, AMSR-E, GPCP
GSMaP_MVK	GSMaP	2000–2014	Hourly	0.10°	IR, TMI, AMSR-E, AMSR, SSMI
MSWEP V1.1	MSWEP	1979–2015	3 hourly	0.25°	CPC Unified, GPCC, CMORPH, GSMaP-MVK, TRMM 3B42RT, ERA-Interim, JRA-55, CHPclim
CN05.1	CN05.1	1961–2015	Daily	0.25°	Gauge

Websites for downloading the datasets. CMORPH_bleneded: http://data.cma.cn/data/cdcdetail/dataCode/SEVP_CLI_CHN_MERGE_CMP_PRE_HOUR_GRID_0.10.html. PERSIANN_CDR: <https://climatedataguide.ucar.edu/climate-data/persiann-cdr-precipitation-estimation-remotely-sensed-information-using-artificial>. TMPA 3B42 V7: <https://pmm.nasa.gov/data-access/downloads/trmm>. GSMaP_MVK: <https://sharaku.eorc.jaxa.jp/GSMaP/index.htm>. MSWEP V1.1: <http://www.gloh2o.org>. CN05.1: http://data.cma.cn/data/cdcdetail/dataCode/SEVP_CLI_CHN_PRE_DAY_GRID_0.25.html.

PERSIANN-CDR is generated from the PERSIANN algorithm using GridSat-B1 IR data and adjusted using the GPCP monthly product. The dataset with spatial and temporal resolutions of 0.25° and daily, respectively, was used in this study [42].

TRMM 3B42 V7 was retrieved by MW and IR signals, and corrected by the gauge data. Passive MW data were first corrected by TMI and PR, and then used to correct the IR data. After combining the MW and IR data, the TRMM Multi-Satellite Precipitation Analysis (TMPA) 3B42 V7 was obtained through the correction of global precipitation data (GPCP). The spatial and temporal resolutions were 0.25° and 3 h, respectively [43].

GSMaP_MVK predicted the precipitation rate from the MW data using the Kalman filtering method, and then the rate was improved based on the relationship between the brightness temperature data and the ground precipitation rate. The spatial and temporal resolutions were 0.1° and 1 h, respectively [44].

MSWEP V1.1 blended multiple data sources, including gauge data, satellite data, and reanalysis data. CHPclim was used as the average of long-term precipitation, and the deviation was corrected. The long-term mean of MSWEP was based on Climate Hazards Group Precipitation Climatology (CHPclim) dataset, which was bias corrected using catch-ratio equations and observation-based estimates of long-term streamflow and potential evaporation. Then, the precipitation anomalies of the gauges, satellites, and reanalysis data were combined using the weighted average method. Finally, CHPclim was temporally downscaled through the precipitation anomaly. The spatial and temporal resolutions were 0.25° and 3 h, respectively [45].

2.3. Methods

By comparing the downscaled precipitation products with observed precipitation, the indexes, e.g., CC, PBIAS, and root mean square error (RMSE), were used to measure the quantitative accuracy at an annual, monthly, and daily scale. The variables were significantly correlated when the CC was higher than 0.7 [46], and the precision was acceptable when the PBIAS value ranged from −10% to 10% [47]. The frequency bias index (FBI), probability of detection (POD), false alarm ratio (FAR) and threat score (TS) were used to evaluate the accuracy in detecting precipitation occurrence. In addition, the annual distribution, interannual variation, and spatial pattern of precipitation were also used to clarify the detection capability:

$$CC = \frac{\sum_{i=1}^n (O_i - \bar{O})(P_i - \bar{P})}{\sqrt{\sum_{i=1}^n (O_i - \bar{O})^2} \sqrt{\sum_{i=1}^n (P_i - \bar{P})^2}}, \quad (1)$$

$$PBIAS = \frac{\sum_{i=1}^n (P_i - O_i)}{\sum_{i=1}^n O_i} \times 100\%, \quad (2)$$

$$RMSE = \sqrt{\frac{\sum_{i=1}^n (P_i - O_i)^2}{n}}, \quad (3)$$

$$FBI = \frac{a + b}{a + c}, \quad (4)$$

$$POD = \frac{a}{a + c}, \quad (5)$$

$$FAR = \frac{b}{a + b}, \quad (6)$$

$$TS = \frac{a}{a + b + c}, \quad (7)$$

where a is the number of hits, b is the number of false alarms, and c is the number of misses. Perfect values were $FBI = 1$, $POD = 1$, $TS = 1$, and $FAR = 0$ [48–51].

3. Results

3.1. Annual Precipitation and Spatial Pattern

The applicability of the precipitation products was interpreted by the CC, RMSE, temporal variation, and spatial pattern of precipitation at an annual scale.

The CCs between the five precipitation products and the observed annual precipitation ranged from -0.61 to 0.99 (Figure 2a). MSWEP and TRMM showed the highest CCs and were significantly correlated with the ground-based rain gauge data with mean values of 0.79 and 0.76 , respectively. The CCs of CMORPH and GSMaP were relatively lower, with the mean values of 0.29 and 0.33 , respectively.

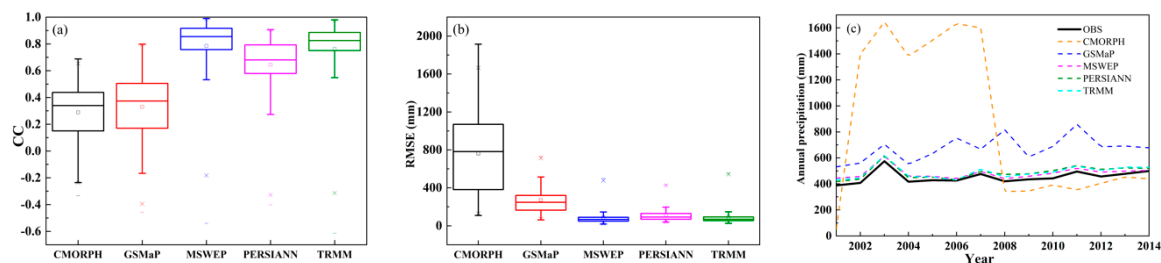


Figure 2. (a) correlation coefficient, (b) root mean square error of annual precipitation between gridded and gauge datasets, and (c) temporal variation of annual precipitation. CC is correlation coefficient, RMSE is root mean square error. (The center line of each boxplot depicts the median value (50th percentile) and the box encompasses the 25th and 75th percentiles of the sample data. The small squares in each boxplot is the arithmetic mean. The whiskers extend from $Q1 - 1.5 \times (Q3 - Q1)$ to $Q3 + 1.5 \times (Q3 - Q1)$, where $Q1$ and $Q3$ are the 25th and 75th percentiles of the sample data, respectively, similarly hereinafter).

The RMSE ranged from 19 mm to 1915 mm (Figure 2b). CMORPH showed the highest RMSE (109–1915 mm) with a mean of 761 mm, followed by GSMaP. The RMSEs of the other three products were relatively lower and ranged from 19 mm to 731 mm. The mean RMSEs of MSWEP and TRMM were the smallest and were similar with values of 88 mm and 89 mm, respectively, thereby indicating that these two products performed better than other datasets, which was consistent with the CC results.

The temporal variation in annual precipitation (Figure 2c) indicated that the observed precipitation showed an upward trend in fluctuation, and the mean ranged from 389 mm to 575 mm. The fluctuating trends and the amount of precipitation estimated by MSWEP, PERSIANN and TRMM were similar to the ground-based rain gauge data, with a range in precipitation between 418 mm and 620 mm. CMORPH and GSMaP demonstrated the largest differences with the ground-based rain gauge data; among them, the precipitation recorded by CMORPH from 2002 to 2007 was above 1380 mm, which was not in line with the actual situation in the Yellow River Basin.

The five products and ground-based rain gauge data showed that the annual precipitation decreased from southeast to northwest (Figure 3), which was consistent with the distribution of climatic conditions in the Yellow River Basin. The contour map of precipitation in the literature showed that the southern part of the Yellow River Basin received the largest amount of precipitation (approximately 700 mm), while the precipitation in the GN in the northwest was reduced to about 200 mm during 1951 to 2001 [52]. The maximum precipitation estimate of CMORPH in the WH was 1400 mm, and there was a 1200 mm high precipitation center in the southern part of the UYR, which was greatly overestimated. The precipitation obtained by GSMaP and PERSIANN in the WH was above 1000 mm, which also overestimated the actual precipitation. The spatial patterns of MSWEP and TRMM were similar to

those in the literature. In addition, the results based on the gauge data in the literature indicated that the average annual precipitation in the Yellow River Basin was 483.7 mm [53], and the average annual precipitation estimated by CMORPH, GSMaP, MSWEP, PERSIANN and TRMM was 853 ± 98 mm, 674 ± 91 mm, 483 ± 44 mm, 489 ± 51 mm, and 491 ± 50 mm, respectively. It could be seen that CMORPH and GSMaP overestimated the precipitation to a larger extent, while the precipitation estimates of MSWEP, PERSIANN and TRMM were close to the values in the literature.

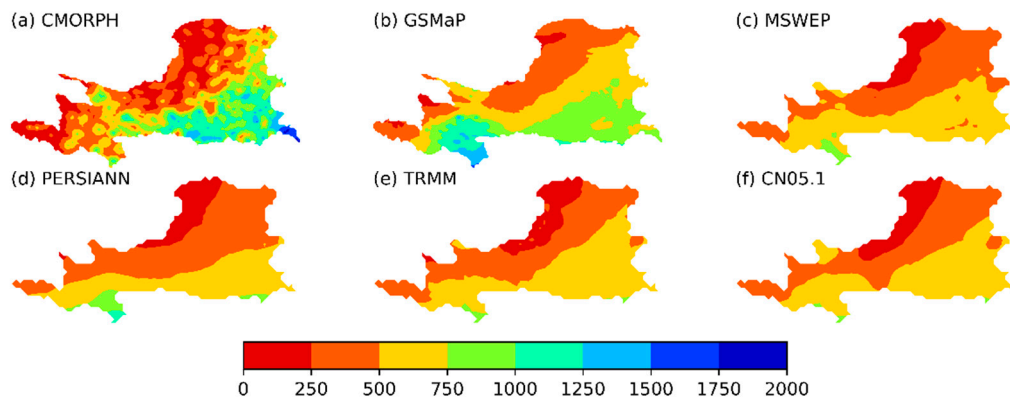


Figure 3. Spatial pattern of annual mean precipitation.

3.2. Monthly Precipitation and Annual Distribution

The CC, RMSE, PBIAS and their distribution during the year were used to interpret the performances of the precipitation products at the monthly scale.

The CCs of the monthly precipitation between the products and the gauge ranged from -0.61 to 0.99 (Figure 4a). More than 97% of the sites from MSWEP, PERSIANN and TRMM were significantly correlated with the ground-based rain gauge data. The CCs of CMORPH and GSMaP were 0.37 – 0.86 and 0.29 – 0.86 , respectively, and 12.9% and 28.7% of the sites were significantly correlated, respectively. MSWEP showed the largest mean CC (0.93), followed by PERSIANN (0.87) and TRMM (0.91), while CMORPH (0.67) and GSMaP (0.63) showed the smallest mean CCs.

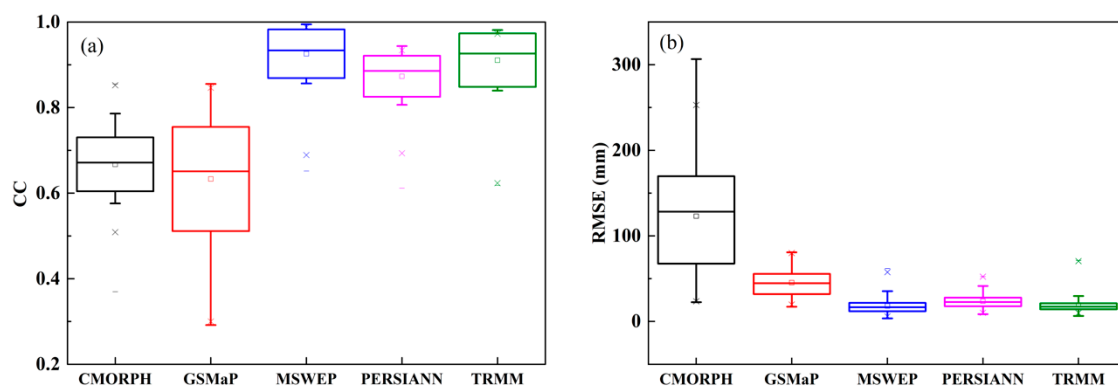


Figure 4. (a) correlation coefficient and (b) root mean square error of monthly precipitation between gridded and gauge datasets. CC is correlation coefficient, RMSE is root mean square error.

CMORPH had the largest RMSE, followed by GSMaP; the ranges were 22.5–307 mm and 17–81 mm and the means were 123 mm and 45.4 mm, respectively. Among the other three precipitation products, MSWEP showed the smallest range and mean RMSE, which were 3.7–62 mm and 18 mm, respectively. PERSIANN showed the largest mean RMSE, which was 23.6 mm (Figure 4b).

The ground-based rain gauge data showed that the monthly precipitation increased from January, reached its peak in July, and then decreased (Figure 5a). The fluctuation trend and amount of

precipitation estimated by MSWEP, PERSIANN and TRMM were close to the ground-based rain gauge data, and the differences ranged from -2.3 mm to 10.5 mm. CMORPH underestimated the precipitation slightly from January to April and from October to December, while it overestimated the precipitation to a large extent from May to September. GSMaP overestimated the precipitation, except for in July and August. The annual distributions of PBIAS, CC and RMSE from MSWEP, PERSIANN and TMPA 3B43 showed higher CCs, lower PBIASs and RMSEs. Their variations were relatively smooth and steady without large fluctuation during the year. CMORPH and GSMaP showed lower CCs, higher PBIASs and RMSEs, and a larger fluctuation range (Figure 5b–d).

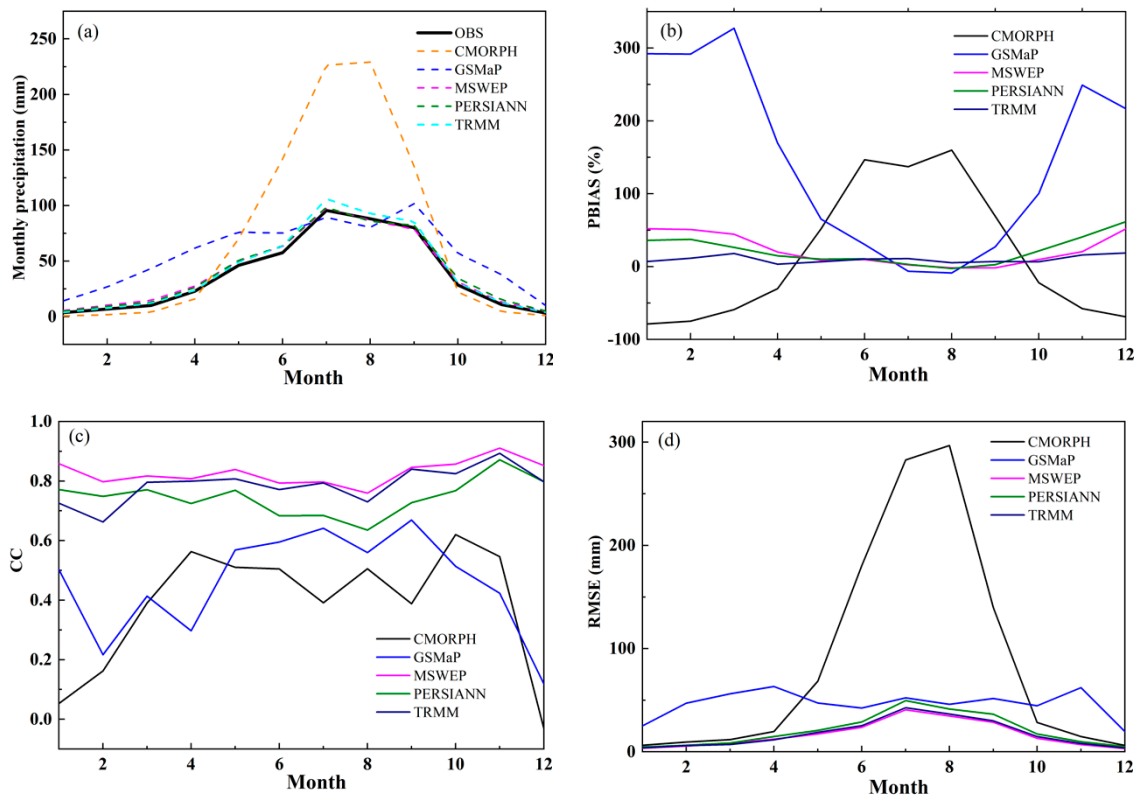


Figure 5. (a) variation of monthly precipitation, (b) PBIAS, (c) correlation coefficient and (d) root mean square error during the year. PBIAS is bias, CC is correlation coefficient, RMSE is root mean square error.

3.3. Daily Precipitation and Precipitation Events

At the daily scale, the assessment was conducted using the precipitation event and the amount of precipitation. The precipitation events were measured by POD, FBI, FAR and TS. The amount of precipitation was quantified by PBIAS, CC and RMSE.

Large differences in the POD among the five precipitation products were observed, as shown in Figure 6a. MSWEP showed the highest POD values, which were all above 0.94 with a mean of 0.97. The POD values of CMORPH, GSMaP and PERSIANN were similar, with a range of 0.6–0.9 and mean of 0.74–0.78. TRMM showed the lowest POD with a range and mean of 0.44–0.85 and 0.64, respectively. From the spatial distribution shown in Figure 7, the PODs of MSWEP at all sites were clearly higher than those of the other four products. CMORPH and GSMaP had higher PODs in the UYR, while PERSIANN showed higher PODs in the FR, WH and WR. TRMM performed relatively poorly in the GN and IM.

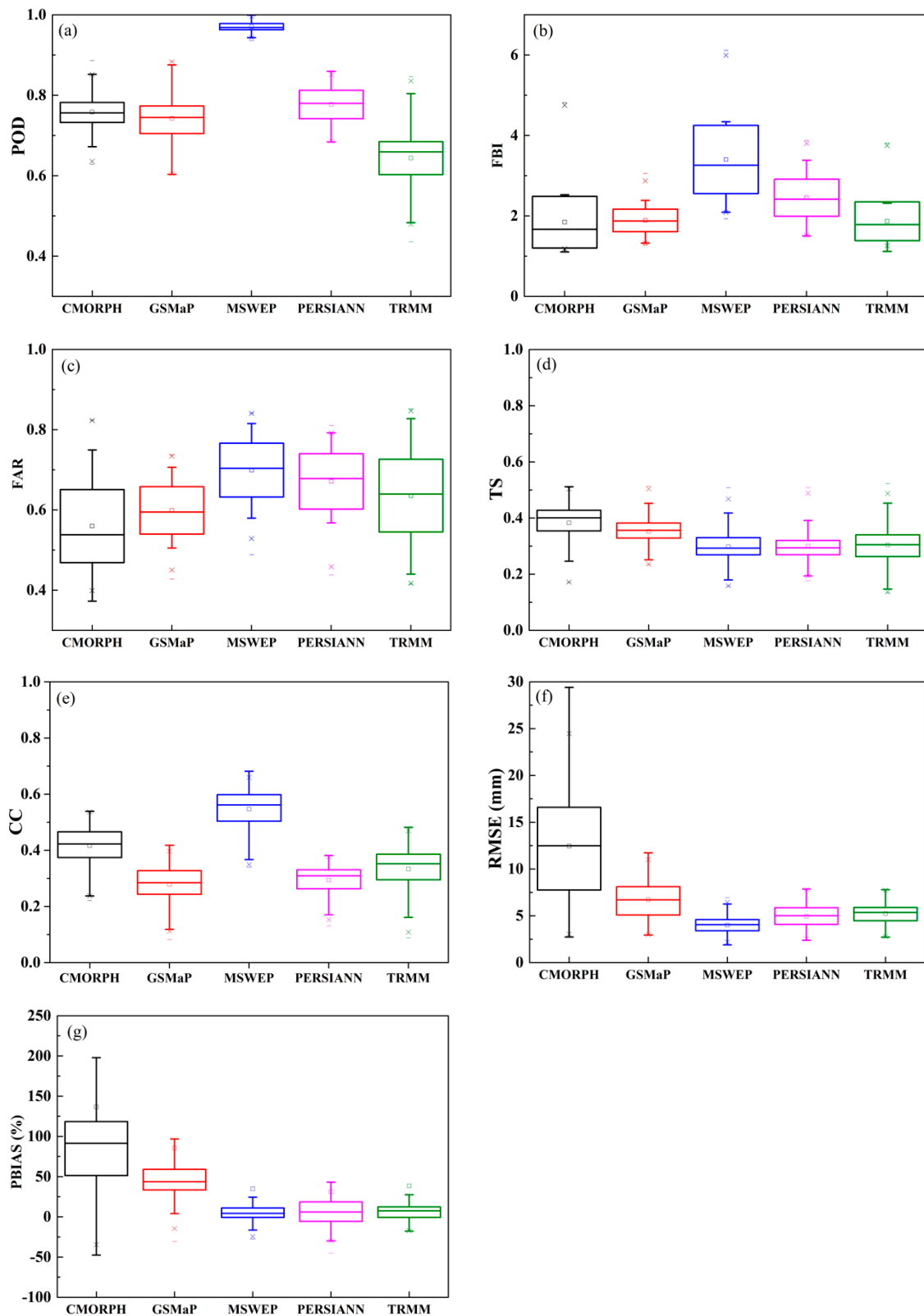


Figure 6. Detective ability of precipitation event: (a) POD, (b) FBI, (c) FAR, (d) TS and detective ability of precipitation: (e) correlation coefficient, (f) root mean square error, (g) PBIAS. POD is probability of detection, FBI is the frequency bias index, FAR is false alarm ratio, CC is correlation coefficient, RMSE is root mean square error, PBIAS is bias.

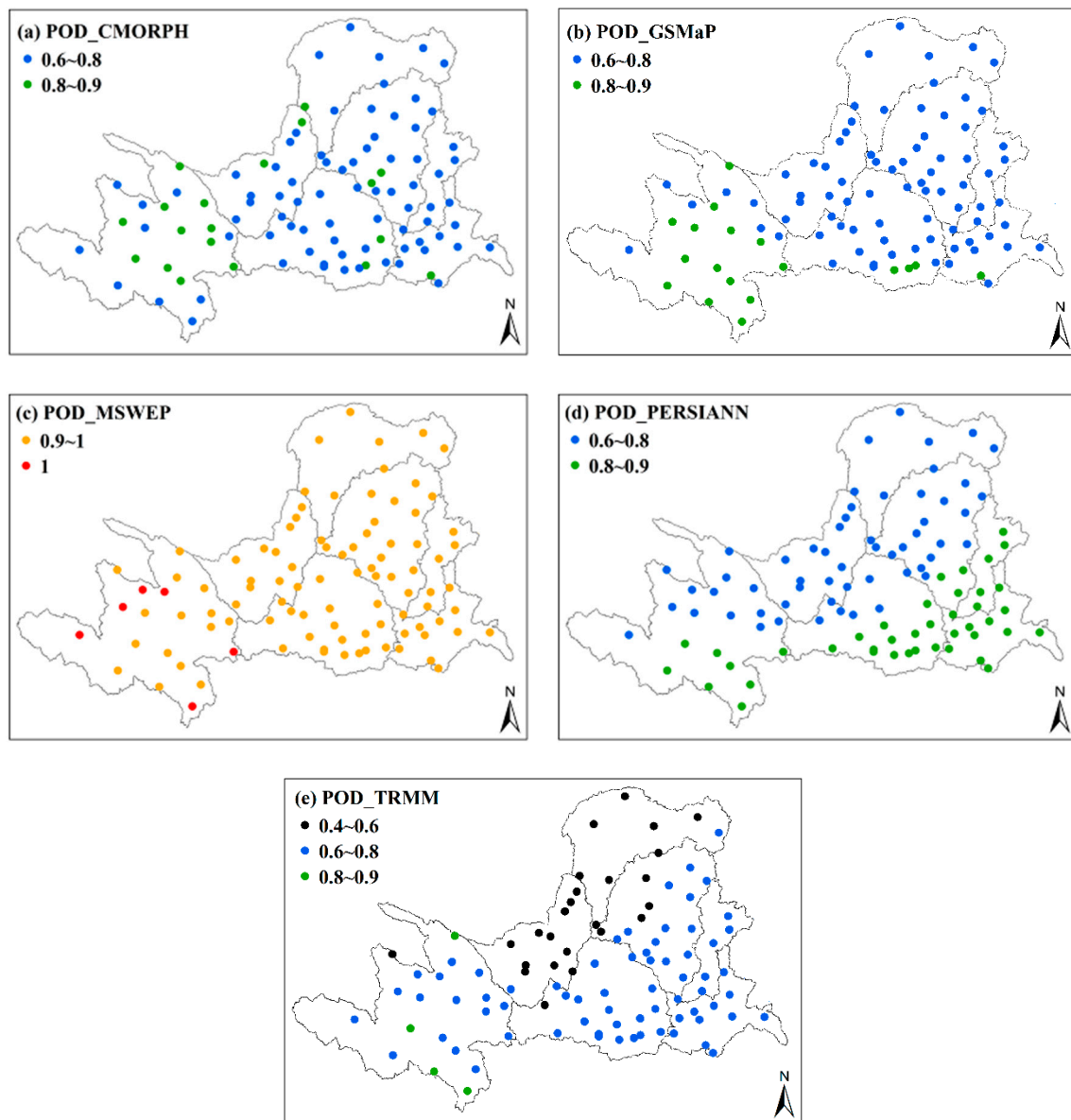


Figure 7. Spatial pattern of POD (probability of detection).

The FBI values of all five products were higher than 1, thereby indicating the overestimation of precipitation occurrence, as shown in Figure 6b. The overestimation degrees of CMORPH, GSMaP and TRMM were relatively lower with FBI values of 1.84, 1.89 and 1.87, respectively. MSWEP showed the highest overestimation degree with a mean FBI value of 3.4. The spatial distribution of the FBI (Figure 8) showed that CMORPH, GSMaP and TRMM had lower overestimation with FBI values ranging from 1 to 2 in the UYR, NSH, FR, WR and WH. MSWEP showed higher overestimation in the GN and IM with FBI values of up to 4 to 6.

As shown in Figure 6c, there were high false alarms and the FAR ranged from 0.37 to 0.85. CMORPH showed the lowest FARs, followed by GSMaP, while MSWEP showed the highest false alarms with mean FARs of 0.56, 0.6 and 0.7, respectively. The FARs of the majority sites were higher than 0.5 (Figure 9). All five products demonstrated that the FARs were highest in the GN, which ranged from 0.7 to 0.9. The FARs of MSWEP were clearly higher than those of the other four products in the IM, NSH, FR and WH.

The TSs of all five precipitation products were lower than 0.52. CMORPH showed the highest TS with a mean of 0.38, followed by GSMaP with a mean of 0.35. MSWEP, PERSIANN and TRMM

showed similar TS, the means were all valued 0.3 (Figure 6d). The spatial distribution of TS showed that CMORPH performed best, while TSs of MSWEP, PERSIANN and TRMM were lower than CMORPH and GSMaP in almost all water system partitions. The TSs also differed in different water system partition. All five precipitation products showed the highest TS in the UYR with the TSs ranged from 0.36 to 0.42, followed by the WR and the WH. The TSs in the GN and IM were the lowest, with the ranges were 0.18–0.27 and 0.22–0.31, respectively (Figure 10).

At the daily scale, all five products were insignificantly correlated with the ground-based rain gauge data (Figure 6e). MSWEP had the highest CCs between 0.34 and 0.68 with a mean of 0.55. The CCs of GSMaP and PERSIANN were the smallest with mean values of 0.28 and 0.29, respectively. As shown in Figure 6f, MSWEP had the smallest RMSE between 1.9 mm and 6.9 mm with a mean of 4 mm. The RMSEs of PERSIANN and TRMM were similar with mean values of 4.9 mm and 5.2 mm, respectively. CMORPH showed the highest RMSE with a mean of 12.5 mm. MSWEP, PERSIANN and TRMM had smaller and more similar PBIASs, with mean values of 34.9%, 31.3% and 38.5%, respectively. CMORPH showed the largest PBIAS ranging from -48% to 2148% with a mean value of 137% (Figure 6g). From the distribution of PBIAS in Figure 11, CMORPH significantly overestimated the daily precipitation at 80% of the stations, and the PBIAS at less than 1% of the stations was within the acceptable range of $\pm 10\%$. GSMaP overestimated the daily precipitation at 97% of the stations, but the overestimation degree was less than that of CMORPH. MSWEP, PERSIANN and TRMM overestimated the daily precipitation at 88% to 93% of the stations. The PBIAS of MSWEP was relatively smaller with values at 65% of stations within the acceptable range, followed by TRMM and PERSIANN with acceptable values at 56% and 45% of the stations, respectively.

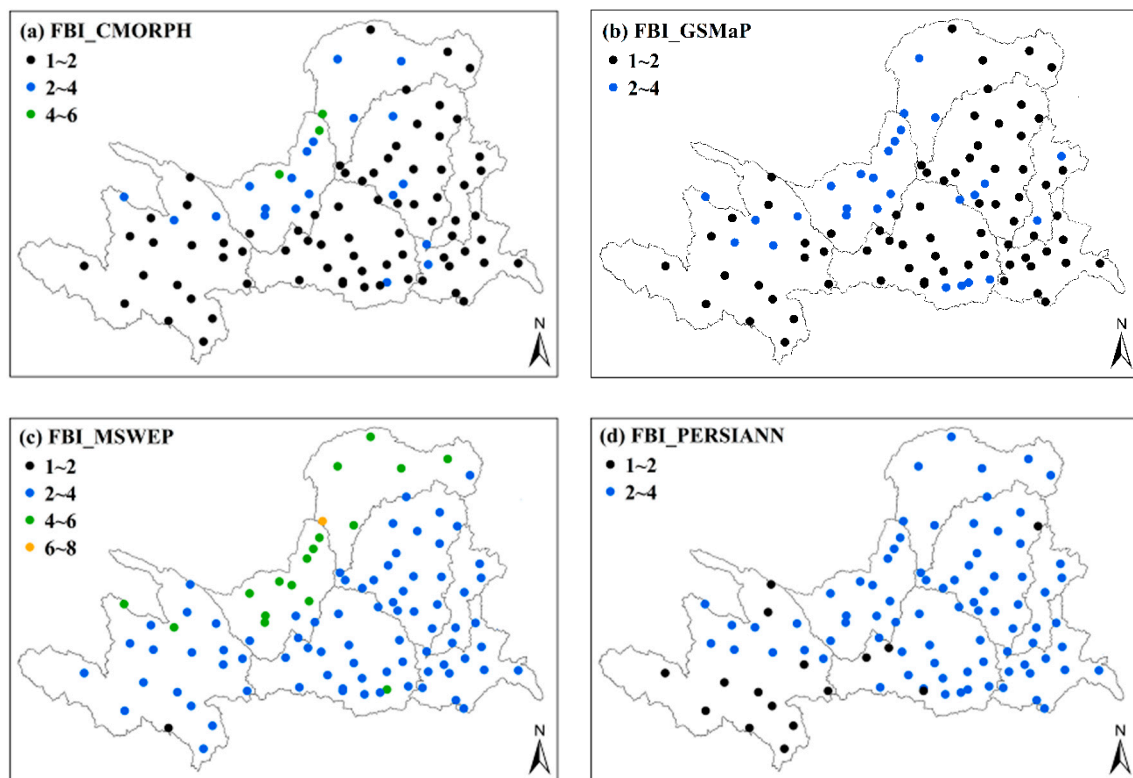


Figure 8. Cont.

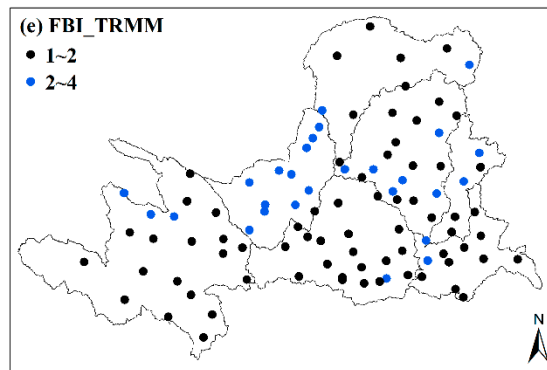


Figure 8. Spatial pattern of FBI (frequency bias index).

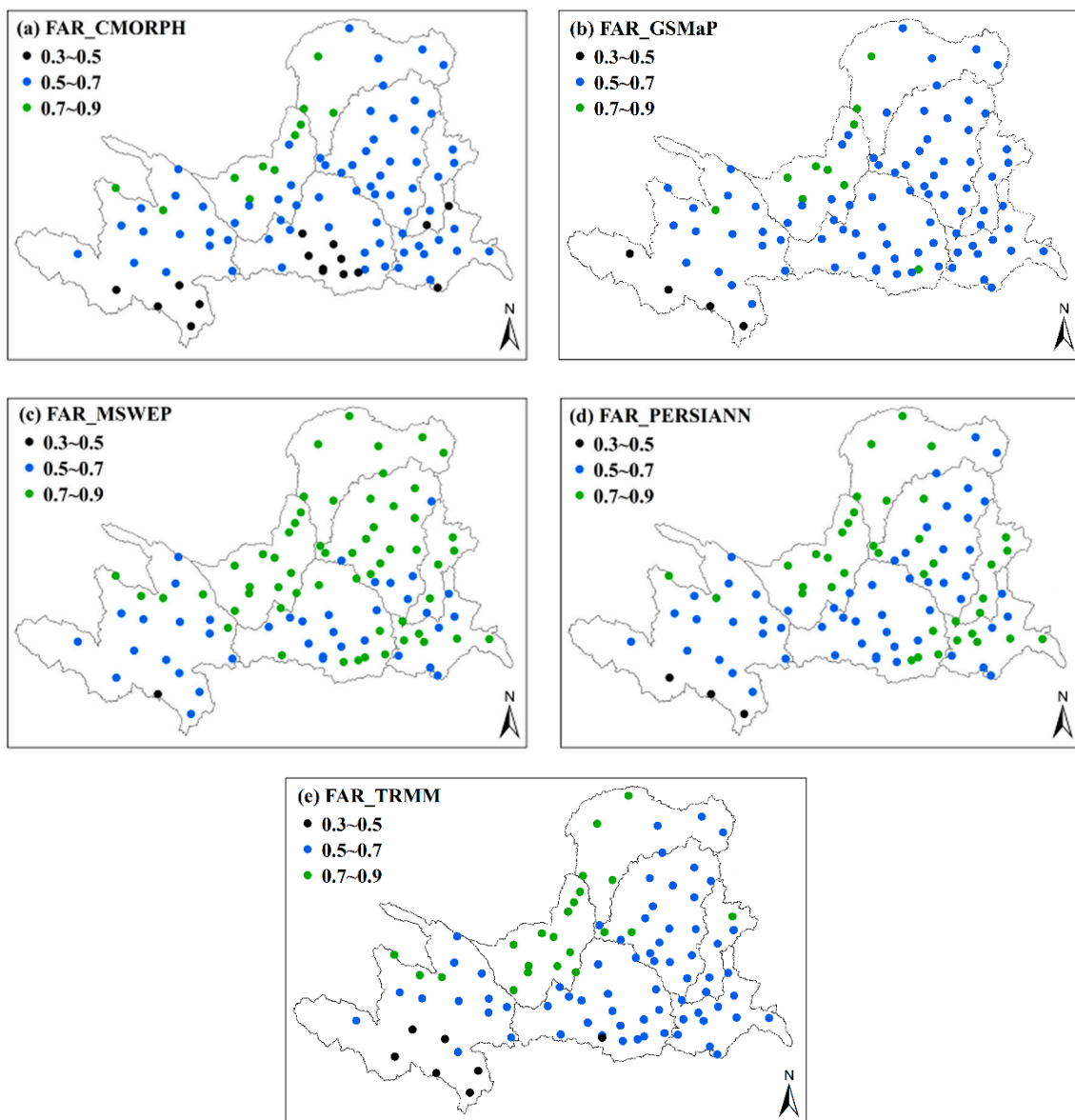


Figure 9. Spatial pattern of FAR (false alarm ratio).

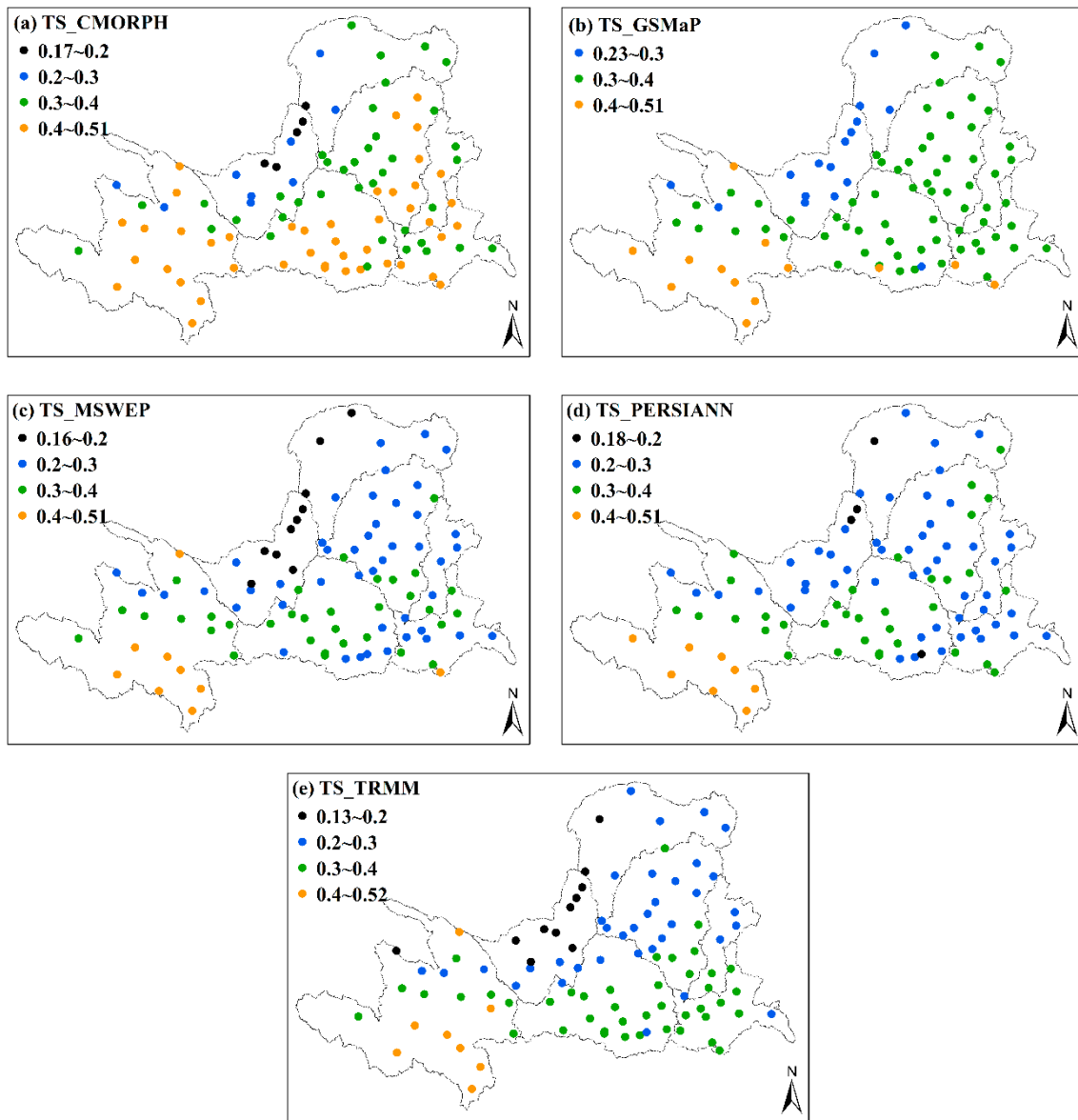


Figure 10. Spatial pattern of TS (threat score).

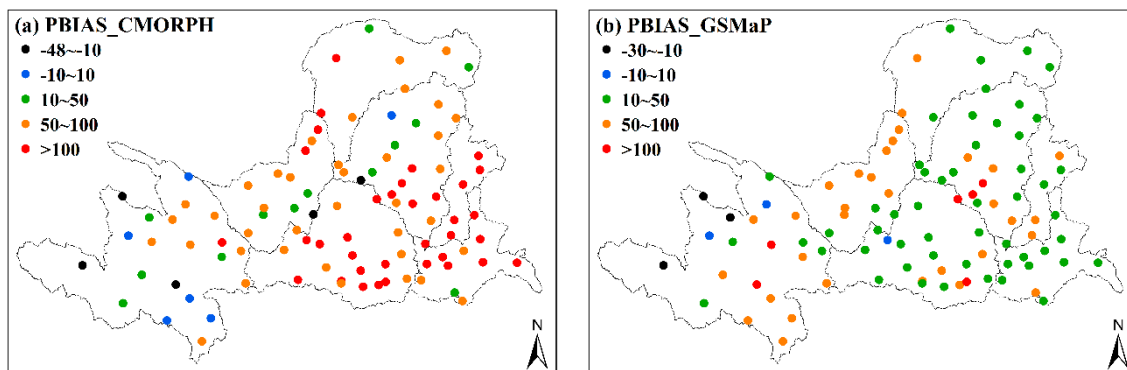


Figure 11. Cont.

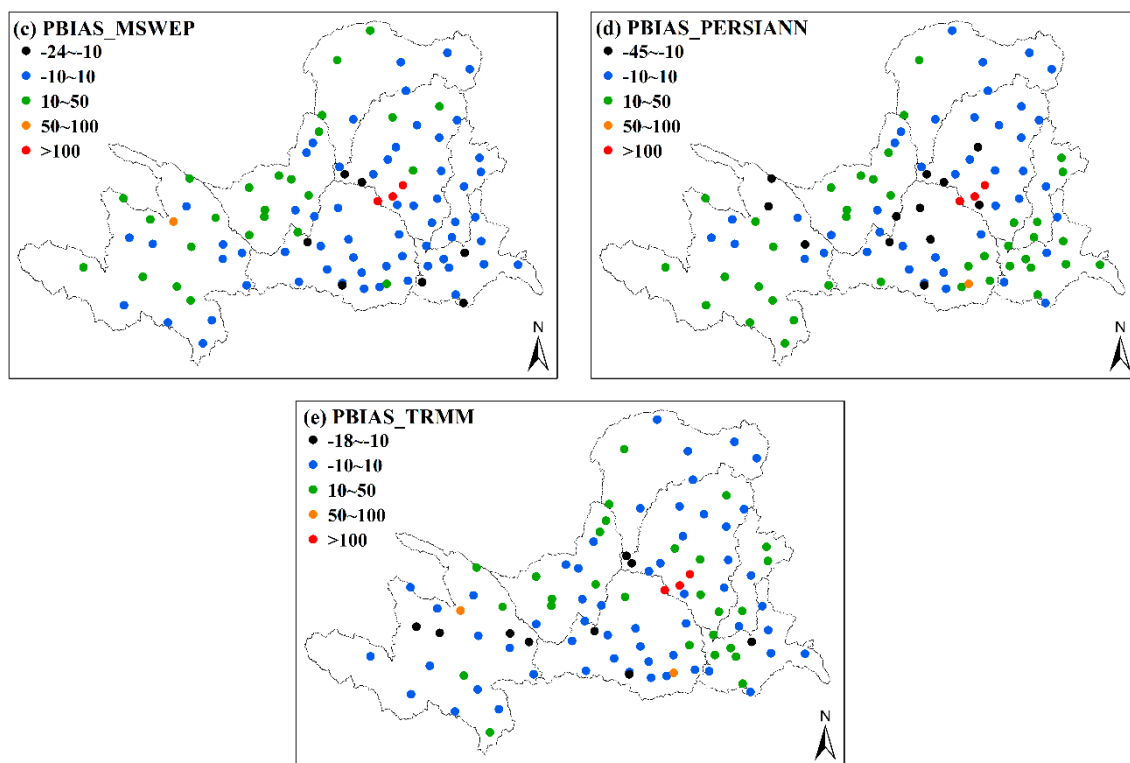


Figure 11. Spatial pattern of PBIAS (bias) on daily scale.

3.4. Frequency Curve of Precipitation

Figure 12a indicates that the precipitation frequency curves of the five products were very similar when the precipitation was above 5 mm/d, and the difference was mainly at precipitation levels below 5 mm/d. All the products underestimated the frequency of dry days, with MSWEP underestimating the frequency to the largest extent (51%), followed by PERSIANN (31%), while CMORPH, GSMaP, and TRMM underestimated the frequency by 17–20%. At the precipitation level of 0–5 mm/d, all the precipitation products overestimated the frequency of precipitation. The degree and rank of overestimation were similar to those of the estimation of dry days.

The PBIAS at different precipitation levels (Figure 12b) showed that all the products overestimated the precipitation at the level of 0–5 mm/d, of which the overestimation was the largest for GSMaP and CMORPH, while it was the smallest for MSWEP. The products underestimated the precipitation above 100 mm/d, with the PBIAS ranging from –85% to –81%, except for CMORPH, which had an acceptable PBIAS. At the level of 5–100 mm/d, all the products underestimated the precipitation, except for the overestimation by CMORPH. The PBIAS increased with the increase in the precipitation level. GSMaP showed the smallest PBIAS at the level of 5–10 mm/d, while CMORPH showed the smallest PBIAS at the level of 10–200 mm/d.

All the precipitation products were insignificantly correlated with the ground-based rain gauge data at each precipitation level, as shown in Figure 12c. There were negative CCs above the precipitation level of 30 mm/d, thereby indicating a decrease in the correlation. The RMSE of the five products showed a gradual increase with the increase in precipitation level. At each precipitation level, CMORPH and MSWEP showed that largest and the smallest RMSE, respectively (Figure 12d).

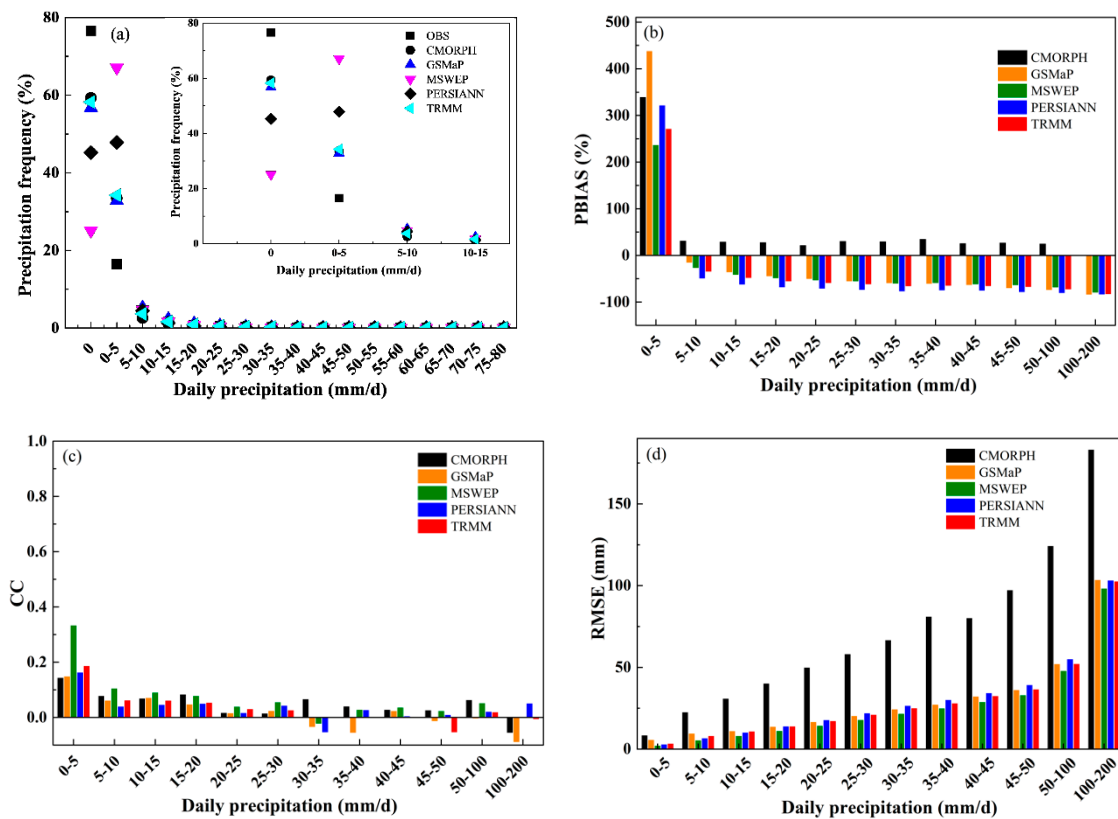


Figure 12. (a) precipitation frequency, (b) PBIAS, (c) correlation coefficient, (d) root mean square error for different precipitation level. PBIAS is bias, CC is correlation coefficient, RMSE is root mean square error.

3.5. Applicability in Sub-Regions

In this section, the applicability of the five precipitation products in 24 sub-basins is discussed. There was no gauge in the Kushui River, Zuli River, or Zhuanglang River, which were not analyzed here.

At the annual scale, Figure 13a,b shows that the CCs of MSWEP and TRMM were higher than 0.7 and were significant, except for in the Beiluo River and the Qingjian River Basin. The RMSEs of these two sub-basins were between 200 mm and 1118 mm, which were higher than those of the other sub-basins. The CCs of CMORPH and GSMaP were lower, while the RMSEs were higher than those of other products.

At the monthly scale, the CCs of the products were higher than 0.7, except for CMORPH and GSMaP. MSWEP showed a higher CC, but the CCs of the Beiluo River and Qingjian River were lower than those of the other sub-basins. CMORPH showed the largest RMSE between 40 mm and 307 mm followed by GSMaP with values between 22 mm and 64 mm; MSWEP showed the smallest RMSE with values between 6.7 mm and 34 mm. The products showed the largest RMSE of 33–64 mm in the Beiluo River and Qingjian River, except for CMORPH, as shown in Figure 13c,d.

At the daily scale, the CCs of the five precipitation products in all sub-regions were below 0.7 (Figure 13e). CMORPH showed the largest RMSE, followed by GSMaP and MSWEP with values of 5.1–29 mm, 4.1–9.5 mm, and 2.5–6.3 mm, respectively. The RMSEs of the Ying River, Qin River, and Yiluo River were greater than those of the other sub-basins (Figure 13f). Both CMORPH and GSMaP overestimated the precipitation, with PBIAS values of 4.8–772% and 18–540%, respectively. The PBIAS values of other products were slightly lower, with values between –23% and 400%. The PBIAS values of MSWEP and TRMM were almost within an acceptable range, except for those in the Beiluo River and Qingjian River (Figure 13g).

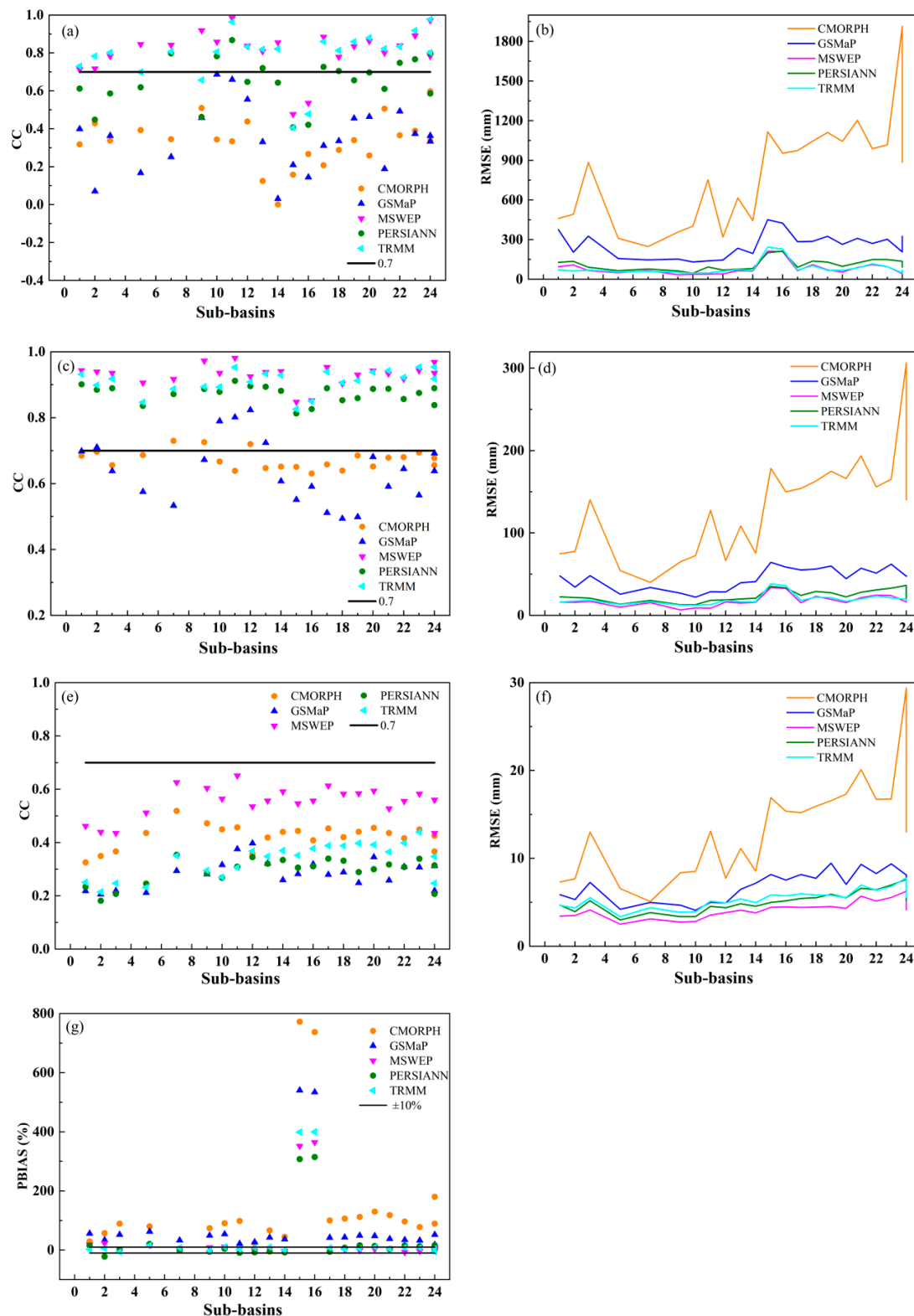


Figure 13. (a) annual correlation coefficient and (b) root mean square error, (c) monthly correlation coefficient and (d) root mean square error, (e) daily correlation coefficient, (f) root mean square error and (g) PBIAS in sub-basins. CC is correlation coefficient, RMSE is root mean square error, PBIAS is bias. (The black line in (a), (c) and (e) means the correlation coefficient is equal to 0.7, above which the variables were significantly correlated. The upper black line in (g), means PBIAS is equal to 10% and the lower black line means PBIAS is equal to -10%, between which the PBIAS is acceptable.)

4. Discussion

4.1. Differences of Data Sources and Algorithms Among Gridded Precipitation Products

The analysis of different temporal and spatial scales showed that MSWEP performed best, followed by TRMM, while CMORPH and GSMaP had the lowest accuracy.

The five types of data were all inferred from MW and IR data, but the data sources and algorithms varied widely. MSWEP combined site, satellite, and reanalysis data, and its data sources were the most diversified. The site density was used as the weight to correct the data, and the influence of terrain was taken into account; thus, the accuracy was higher than that of other satellite data [45]. TRMM combined IR and MW data, and was corrected by site data [43]; however, there were fewer data sources than those used by MSWEP. In the deriving process of PERSIANN, the hourly precipitation data were trained first, and then the parameters were inserted into all the history records. Although the GPCP monthly precipitation data were used for correction [54,55], passive MWs, which were valuable for deriving precipitation, were not combined in the algorithms, and IR signals were mainly used.

The CMORPH precipitation product, which was developed by the CPC of NCEP, derived the precipitation using a tracking method. The main data source was passive MW data, while IR data were only used indirectly to derive the cloud field. Although IR data were less accurate, they could provide useful information when passive MWs were not available. In addition, assuming that the rain intensity was a constant was unreasonable in the forward and backward propagation of MW estimation [56], which might have resulted in lower accuracy of the original CMORPH. On the basis of this product, an hourly blended precipitation product was developed using probability density function matching and the optimal interpolation method to combine the site data with the original grid data. The site data used in this product were hourly precipitation data from an automatic meteorological station; the measurements were stopped in winter and the precipitation was valued as 0, which might have been the main reason for the low accuracy of the product.

Similar to the original CMORPH, GSMaP used the MORPHing technique to derive the cloud motion vectors [40]. The difference was that GSMaP used the new Kalman filter to assimilate the IR precipitation rate, which helped to reduce the total error of the Kalman filter method even though the accuracy was lower than that derived from the passive MW data. On the other hand, GSMaP did not adopt standardization like CMORPH in merging passive MWs [6]. Moreover, GSMaP was not corrected by the gauge data, and a systematic error existed in the pure satellite product [57]. In summary, using multiple reliable data sources and correcting the data using gauge data could help to improve the accuracy of the precipitation products.

4.2. Results Comparison with Previous Studies

This study showed that MSWEP overestimated the daily precipitation overall, which was consistent with its performance over mainland China and Qinghai-Tibet Plateau [23,58]. MSWEP overestimated the light precipitation, while underestimating the heavy precipitation in the Yellow River Basin; this result was consistent with its performance over mainland China [23]. In addition, the monthly and daily correlation coefficient in the Yellow River Basin was 0.93 and 0.55, respectively, which was close to that of mainland China (0.94 and 0.57, respectively). It was reported that POD and FAR of MSWEP in the Qinghai-Tibet Plateau was 0.65 and 0.5, respectively [58]. In this study, POD was 0.97 and FAR was 0.7, which means that MSWEP showed better probability of detection but higher false alarms in the Yellow River Basin than that in Qinghai-Tibet Plateau. The consistency between daily precipitation of MSWEP and rain gauge observation was relatively low in mainland China [23]. However, comparing with other four precipitation products, MSWEP performed best in the Yellow River Basin with higher CC and POD, lower PBIAS and RMSE, although it showed higher FBI and FAR.

Previous studies showed that the precision of TRMM increased with the increase of time scale [59]. In this study, however, TRMM performed best on monthly scale with the correlation coefficient was

0.91, followed by annual scale with the correlation coefficient was 0.76, and daily scale with the correlation coefficient was 0.33. This result was consistent with that of Lancang River Basin [60]. It was indicated by several studies that TRMM performed better in humid regions than in arid area [59,61], but there was no obvious regional difference in the Yellow River Basin. The correlation coefficient on daily scale reach up to 0.79, FAR was 0.14 over China [62], but the performance of TRMM in the Yellow River Basin was lower than that in China, the correlation coefficient and FAR valued 0.33 and 0.64, respectively. This study found that TRMM outperformed than CMORPH, PERSIANN and GSMaP, which was consistent with that in Ganjiang River Basin and Circum-Bohai-Sea Region [63].

PERSIANN tended to underestimate the daily precipitation in Oujiang Basin and Circum-Bohai-Sea Region [64], but it overestimated the precipitation with the PBIAS of 31.3% in this study. PERSIANN underestimated the precipitation for all rainfall levels in Oujiang Basin [64]. However, it overestimated the precipitation when the precipitation was below 5 mm/d and the situation was opposite when the precipitation was above 5 mm/d in the Yellow River Basin. PERSIANN underestimated monthly precipitation overall and underestimated the seasonal precipitation except winter in Circum-Bohai-Sea Region [65]. In the Yellow River, the precipitation was overestimated overall, and the precipitation was overestimated from October to April, while the precision in other months could be acceptable. Previous study indicated that PERSIANN was more applicable for areas with less precipitation [66]; this study also found that there was a higher POD in wetter regions such as WR, WH and FR.

CMORPH could reflect spatial patterns of precipitation and capture the rainstorm in some local areas such as Shaanxi Province and Circum-Bohai-Sea Region in China [65,67]. However, majority studies indicated that CMORPH performed poorly in describing temporal variation and spatial distribution of precipitation [68,69]. In this study, CMORPH also had difficulty in estimating precipitation pattern, which demonstrated that the precipitation was seriously overestimated spatially and temporally. It was reported that CMORPH had large biases in detecting heavy rain in Shaanxi Province and Circum-Bohai-Sea Region [65,67], and underestimated the precipitation for all rainfall levels in Oujiang Basin [64]. However, the PBIAS was positive for almost all rainfall levels, and was the highest for the precipitation of 0–5 mm/d, but was relatively lower for the precipitation higher than 5 mm/d, indicating that CMORPH was prone to overestimate the precipitation and had more difficulty in estimating light precipitation in the Yellow River Basin. From the perspective of precipitation events, there was a large amount of false alarms and the maximum reach up to 0.9 in China. The false alarms in southeast China were lower than that in northwest part [68]. This study also showed FARs decreased from southeast to northwest in the Yellow River Basin, but they ranged from 0.37 to 0.82 and were the lowest compared to other four precipitation products. The monthly and annual correlation coefficient was 0.89 and 0.77 in Lancang River Basin [60], and the value was much lower in the Yellow River Basin (0.67 and 0.29, respectively). Seasonally, CMORPH performed better in detecting summer precipitation in five provinces of China and Tianshan region [66,70]; it also overestimated the summer precipitation but underestimated winter precipitation in Tianshan region [70], the same was true for the Yellow River Basin.

GSMaP performed differently in different regions. There was an obvious overestimation in areas with less precipitation, but the situation is opposite in areas with more precipitation in Hunan Province [71]. The contribution of false alarms and omissions to the overall bias was close to each other and cancelled each other out, resulting in lower overall bias and better performance [71]. GSMaP overestimated the summer precipitation in Sichuan, especially in mountainous area with complex terrain [72], but generally underestimated precipitation in Poyang Lake Basin [73]. However, in the Yellow River Basin of this study, precipitation from 95% of stations was overestimated, and precipitation was overestimated except July and August, false alarms were four times more than omissions was responsible for the overestimation for the whole basin. In addition, it was reported that monthly and daily correlation coefficients in Poyang Lake Basin was 0.85 and 0.5 on average [73], but they were much lower and valued 0.63 and 0.28 in the Yellow River Basin, respectively.

4.3. Hydrological Application of the Gridded Precipitation Products

The gridded precipitation products were widely used in hydrology, especially in the aspect of runoff simulation, flood prediction and drought monitoring.

TRMM showed better applicability than CMORPH in simulating runoff in Lancang River Basin, Nu Basin, Ganges, Brahmaputra and Meghna Basins [60,74,75]. In humid regions of China, TRMM 3B42 could better predict daily runoff, while PERSIANN was inclined to underestimate large runoff. PERSIANN also tended to underestimate extreme precipitation and extreme runoff, while overestimation and underestimation of extreme precipitation and runoff coexist for TRMM 3B42 [16]. Comparing with Global Precipitation Measurement (GPM) and IMERG, GSMaP showed the best performance in simulating hourly runoff, the generated flood map also agreed with the published information. It is capable to support rapid flood forecasting required for early warning of floods [76].

Using MSWEP and TRMM as the forcing data provided satisfactory results for conceptual HBV-96 model, while PERSIANN led to better prediction of flow peaks but overestimations of the hydrographs' falling limbs in the Brahmaputra basin [77]. Fallah and Orth [78] found that the accuracy of precipitation inputs had significant influence on simulated runoff, and MSWEP yield good performance in European catchments. Patricia [79] calibrated the large-scale hydrological model PCRaster GLOBal Water Balance (PCR-GLOBWB) using three global precipitation products (ERA-Interim, WFDEI and MSWEP) in the Moroccan Oum er Rbia River basin. The result showed that precipitation input affected discharge estimates more than calibrating model parameters. WFDEI led to the lowest model performances. The highest discharge improvement was obtained when ERA-Interim and MSWEP were used in combination. In India, TRMM, Global Data Assimilation System (GDAS), CHIRPS and MSWEP were used as meteorological forcing in Noah 3.6 LSM for simulating soil moisture. The results showed that the simulated soil moisture forced by GDAS and MSWEP consistently outperformed the other simulation outputs [80]. MSWEP provided a greater potential for drought monitoring over western China than CMORPH and TRMM. It was found that MSWEP based Standardized Precipitation Index (SPI) could not only precisely reflect the occurrence and development of drought events, but also reasonably describe important characteristics of typical drought events. Generally, MSWEP could be used as an alternative data for drought monitoring over mainland China, particularly in eastern China, but improvement was required in the arid and semi-arid regions of western China [81].

From above, various gridded precipitation products provided alternative data sources and performed differently for hydrology. Overall, MSWEP showed a great potential applicability. However, the limitation of this study was that the hydrological application was not investigated, which will be our next steps.

5. Conclusions

Five precipitation products were evaluated at multiple temporal and spatial scales from 2001 to 2014 in the Yellow River Basin of China, and the conclusions were as follows:

(1) For precipitation events, MSWEP and TRMM showed the highest and lowest POD, respectively. MSWEP and CMORPH had the highest and the lowest FARs, respectively. The difference in precipitation frequency of the five precipitation products was mainly reflected at the precipitation level below 5 mm/d. All the products underestimated the frequency of dry days and overestimated the precipitation frequency; however, they overestimated its amount at the precipitation level of 0–5 mm/d. The performance of CMORPH and GSMaP showed opposite trends.

(2) For precipitation, MSWEP was significantly correlated with the ground-based rain gauge data, and showed the lowest RMSE and PBIAS at the monthly and annual scales. CMORPH and GSMaP showed the lowest CCs and the highest RMSEs and PBIASs.

(3) The annual distribution patterns, interannual variations, and spatial patterns of averaged annual precipitation of MSWEP and TRMM were similar to the observed values, while those of CMORPH and GSMaP were significantly different from the ground-based rain gauge data.

(4) At the sub-basin scale, MSWEP performed best. All five precipitation products performed poorly in the Beiluo River and Qingjian River, and were more applicable in other sub-basins.

Author Contributions: Conceptualization, Y.Y.; methodology, Y.Y., L.B. and B.W.; validation, J.W., L.B. and B.W.; formal analysis, Y.Y. and J.W.; writing—original draft preparation, Y.Y. writing—review and editing, L.B. and B.W.; supervision, B.W.; funding acquisition, Y.Y. All authors have read and agreed to the published version of the manuscript.

Funding: This research was funded by the National Key Research and Development Program of China, 2016YFC0501603, and the Chinese Academy of Sciences “Light of West China” Program.

Conflicts of Interest: The authors declare no conflict of interest.

References

1. Duncan, M.; Austin, B.; Fabry, F.; Austin, G. The effect of gauge sampling density on the accuracy of streamflow prediction for rural catchments. *J. Hydrol.* **1993**, *142*, 445–476. [[CrossRef](#)]
2. Wilk, J.; Kniveton, D.; Andersson, L.; Layberry, R.; Todd, M.C.; Hughes, D.; Ringrose, S.; Vanderpost, C. Estimating rainfall and water balance over the Okavango River Basin for hydrological applications. *J. Hydrol.* **2006**, *331*, 18–29. [[CrossRef](#)]
3. Bell, T.; Abdullah, A.; Martin, R.; North, G. Sampling errors for satellite-derived tropical rainfall- Monte Carlo study using a space-time stochastic model. *J. Geophys. Res.* **1990**, *95*, 2195–2205. [[CrossRef](#)]
4. Bowman, K.P. Comparison of TRMM precipitation retrievals with rain gauge data from ocean buoys. *J. Clim.* **2005**, *18*, 178–190. [[CrossRef](#)]
5. Kummerow, C. Beamfilling errors in passive microwave rainfall retrievals. *J. Appl. Meteorol.* **1998**, *37*, 356–370. [[CrossRef](#)]
6. Tian, Y.D.; Peters-Lidard, C.D.; Adler, R.F.; Kubota, T.; Ushio, T. Evaluation of GSMaP precipitation estimates over the contiguous United States. *J. Hydrometeorol.* **2010**, *11*, 566–574. [[CrossRef](#)]
7. Li, J.; Heap, A.D. *A Review of Spatial Interpolation Methods for Environmental Scientists*; Geoscience Australia: Canberra, Australia, 2008.
8. Scheel, M.L.M.; Rohrer, M.; Huggel, C.; Santos Villar, D.; Silvestre, E.; Huffman, G.J. Evaluation of TRMM Multi-satellite Precipitation Analysis (TMPA) performance in the Central Andes region and its dependency on spatial and temporal resolution. *Hydrol. Earth Syst. Sci. Discuss.* **2011**, *15*, 2649–2663. [[CrossRef](#)]
9. Duethmann, D.; Zimmer, J.; Gafurov, A.; Güntner, A.; Merz, B.; Vorogushyn, S. Evaluation of areal precipitation estimates based on downscaled reanalysis and station data by hydrological modelling. *Hydrol. Earth Syst. Sci. Discuss.* **2012**, *9*, 10719–10773. [[CrossRef](#)]
10. Tobin, C.; Nicotina, L.; Parlange, M.B.; Berne, A.; Rinaldo, A. Improved interpolation of meteorological forcings for hydrologic applications in a Swiss Alpine region. *J. Hydrol.* **2011**, *401*, 77–89. [[CrossRef](#)]
11. Beck, H.E.; Vergopolan, N.; Pan, M.; Levizzani, V.; Van Dijk, A.; Weedon, G.P.; Brocca, L.; Huffman, G.J.; Wood, E.F.; William, L. Global-scale evaluation of 22 precipitation datasets using gauge observations and hydrological modeling. *Hydrol. Earth Syst. Sci. Discuss.* **2017**, *21*, 1–23. [[CrossRef](#)]
12. Cheng, L.; Shen, R.P.; Shi, C.X.; Bai, L.; Yang, Y.H. Evaluation and verification of CMORPH and TRMM 3B42 precipitation estimation products. *Meteorological* **2014**, *40*, 1372–1379.
13. Guo, H.; Chen, S.; Bao, A.M.; Hu, J.J.; Yang, B.H.; Stepanian, P. Comprehensive Evaluation of High-Resolution Satellite-Based Precipitation Products over China. *Atmosphere* **2016**, *7*, 6. [[CrossRef](#)]
14. Li, C.M.; Tang, G.Q.; Hong, Y. Cross-Evaluation of Ground-based, Multi-Satellite and Reanalysis Precipitation Products: Applicability of the Triple Collocation Method across Mainland China. *J. Hydrol.* **2018**, *562*, 71–83. [[CrossRef](#)]
15. Zhao, H.G.; Yang, B.G.; Yang, S.T.; Huang, Y.C.; Dong, G.T.; Bai, J.; Wang, Z.W. Systematical estimation of GPM-based global satellite mapping of precipitation products over China. *Atmos. Res.* **2018**, *201*, 206–217. [[CrossRef](#)]
16. Zhu, Q.; Xuan, W.D.; Liu, L.; Xu, Y.P. Evaluation and hydrological application of precipitation estimates derived from PERSIANN-CDR, TRMM 3B42V7 and NCEP-CFSR over humid regions in China. *Hydrol. Process.* **2016**, *30*, 3061–3083. [[CrossRef](#)]

17. Zhang, S.J.; Wang, D.H.; Qin, Z.K.; Zheng, Y.Y.; Guo, J.P. Assessment of the GPM and TRMM Precipitation Products Using the Rain Gauge Network over the Tibetan Plateau. *J. Meteorol. Res.* **2018**, *32*, 324–336. [[CrossRef](#)]
18. Gao, Y.C.; Liu, M.F. Evaluation of high-resolution satellite precipitation products using rain gauge observations over the Tibetan Plateau. *Hydrol. Earth Syst. Sci. Discuss.* **2013**, *17*, 837–849. [[CrossRef](#)]
19. Tong, K.; Su, F.G.; Yang, D.Q.; Hao, Z.C. Evaluation of satellite precipitation retrievals and their potential utilities in hydrologic modeling over the Tibetan Plateau. *J. Hydrol.* **2014**, *519*, 423–437. [[CrossRef](#)]
20. Zhu, H.L.; Li, Y.; Huang, Y.W.; Li, Y.C.; Hou, C.C.; Shi, X.L. Evaluation and hydrological application of satellite-based precipitation datasets in driving hydrological models over the Huifa river basin in Northeast China. *Atmos. Res.* **2018**, *207*, 28–41. [[CrossRef](#)]
21. Chen, C.; Chen, Q.W.; Duan, Z.; Zhang, J.Y.; Mo, K.L.; Li, Z.; Tang, G.Q. Multiscale Comparative Evaluation of the GPM IMERG v5 and TRMM 3B42 v7 Precipitation Products from 2015 to 2017 over a Climate Transition Area of China. *Remote Sens.* **2018**, *10*, 944. [[CrossRef](#)]
22. Gao, F.; Zhang, Y.H.; Chen, Q.H.; Wang, P.; Yang, H.R.; Yao, Y.J.; Cai, W.Y. Comparison of two long-term and high-resolution satellite precipitation datasets in Xinjiang, China. *Atmos. Res.* **2018**, *212*, 150–157. [[CrossRef](#)]
23. Deng, Y.; Jiang, W.G.; Wang, X.Y.; Lyu, J.X. Accuracy assessment of MSWEP over mainland China. *Adv. Water Sci.* **2018**, *29*, 455–464. (In Chinese)
24. Miao, C.Y.; Ashouri, H.; Hsu, K.L.; Sorooshian, S.; Duan, Q.Y. Evaluation of the PERSIANN-CDR Daily Rainfall Estimates in Capturing the Behavior of Extreme Precipitation Events over China. *J. Hydrometeorol.* **2015**, *16*, 1387–1396. [[CrossRef](#)]
25. Liu, X.M.; Yang, T.T.; Hsu, K.L.; Liu, C.M.; Sorooshian, S. Evaluating the streamflow simulation capability of PERSIANN-CDR daily rainfall products in two river basins on the Tibetan Plateau. *Hydrol. Earth Syst. Sci. Discuss.* **2017**, *21*, 1–31. [[CrossRef](#)]
26. Li, Q.L.; Zhang, W.C.; Yi, L.; Liu, J.P.; Chen, H. Accuracy evaluation and comparison of GPM and TRMM precipitation product over Mainland China. *Adv. Water Sci.* **2018**, *29*, 303–313. (In Chinese)
27. Collischonn, B.; Collischonn, W.; Tucci, C.E.M. Daily hydrological modeling in the Amazon basin using TRMM rainfall estimates. *J. Hydrol.* **2008**, *360*, 207–216. [[CrossRef](#)]
28. Dong, G.T.; Fan, D.; Yang, S.T.; Xue, H.Z.; Zhou, J.L.; Dang, S.Z.; Cheng, C.X. Analysis on the Applicability of GPM and TRMM Precipitation Data in the Yellow River Basin. *Res. Soil Water Conserv.* **2018**, *25*, 81–87. (In Chinese)
29. Li, F.X.; Chen, D.; Tang, Q.H. Variations of hydro-meteorological variables in the Yellow River basin and their relationships with the East Asian summer monsoon. *Adv. Water Sci.* **2015**, *26*, 481–490. (In Chinese)
30. Mai, M.; Zeng, Y.; Qiu, X.F. Variation of Sunshine Percentage for the Last 40 Years in the Yellow River Basin. *Meteorological* **2006**, *32*, 62–66. (In Chinese)
31. He, J.P.; He, Z. Spatio-temporal characteristics of extreme precipitation event in Yellow River basin in recent 53 a. *Ecol. Environ. Sci.* **2014**, *23*, 95–100. (In Chinese)
32. Wu, J.; Gao, X.J. A gridded daily observation dataset over China region and comparison with the other datasets. *Chin. J. Geophys.* **2013**, *56*, 1102–1111. (In Chinese)
33. New, M.; Lister, D.; Hulme, M. A high-resolution data set of surface climate over global land areas. *Clim. Res.* **2002**, *21*, 1–25. [[CrossRef](#)]
34. Xie, P.P.; Yatagai, A.; Chen, M.Y.; Hayasaka, T.; Fukushima, Y.; Liu, C.M.; Yang, S. A Gauge-based analysis of daily precipitation over East Asia. *J. Hydrometeorol.* **2007**, *8*, 607–626. [[CrossRef](#)]
35. Xu, Y.; Gao, X.J.; Shen, Y.; Xu, C.; Shi, Y.; Giorgi, F. A daily temperature dataset over China and its application in validating a RCM simulation. *Adv. Atmos. Sci.* **2009**, *26*, 763–772. [[CrossRef](#)]
36. Yatagai, A.; Arakawa, O.; Kamiguchi, K. A 44-year daily gridded precipitation dataset for Asia based on a dense network of rain gauges. *SOLA* **2009**, *5*, 137–140. [[CrossRef](#)]
37. Zhao, Z.P.; Liu, J.Y.; Shao, Q.Q. Spatial diversity of humidification and its impact on ecosystem vulnerability in China during the last 30 years. *J. Nat. Resour.* **2010**, *25*, 2091–2100. (In Chinese)
38. Gribbon, K.T.; Bailey, D.G. A Novel Approach to Real-time Bilinear Interpolation. In Proceedings of the Second IEEE International Workshop on Electronic Design, Test and Applications, Perth, Australia, 28–30 January 2004; p. 126.
39. Ji, X.; Chen, Y.F. Characterizing spatial patterns of precipitation based on corrected TRMM 3B43 data over the mid Tianshan Mountains of China. *J. Mt. Sci.* **2012**, *9*, 628–645. [[CrossRef](#)]

40. Joyce, R.J.; Janowiak, J.E.; Arkin, P.A.; Xie, P. CMORPH: A method that produces global precipitation estimates from passive microwave and infrared data at high spatial and temporal resolution. *J. Hydrometeorol.* **2004**, *5*, 487–503. [[CrossRef](#)]
41. Shen, Y.; Zhao, P.; Pan, Y.; Yu, J.J. A high spatiotemporal gauge-satellite merged precipitation analysis over China. *J. Geophys. Res. Atmos.* **2014**, *119*, 3063–3075. [[CrossRef](#)]
42. Ashouri, H.; Hsu, K.L.; Sorooshian, S.; Dan, K.B.; Knapp, K.R.; Cecil, L.D.; Nelson, B.R.; Prat, O.P. PERSIANN-CDR: Daily Precipitation Climate Data Record from Multisatellite Observations for Hydrological and Climate Studies. *Bull. Am. Meteorol. Soc.* **2014**, *96*, 197–210. [[CrossRef](#)]
43. Huffman, G.J.; Bolvin, D.T.; Nelkin, E.J.; Wolff, D.B.; Adler, R.F.; Gu, G.; Hong, Y.; Bowman, K.P.; Stocker, E.F. The TRMM multisatellite precipitation analysis (TMPA): Quasi-global, multiyear, combined-sensor precipitation estimates at fine scales. *J. Hydrometeorol.* **2007**, *8*, 38–55. [[CrossRef](#)]
44. Iguchi, T.; Kozu, T.; Kwiatkowski, J.; Meneghini, R.; Awaka, J.; Okamoto, K. A Kalman filter approach to the Global Satellite Mapping of Precipitation (GSMaP) from combined passive microwave and infrared radiometric data. *J. Meteorol. Soc. Jpn.* **2009**, *87A*, 137–151.
45. Beck, H.E.; Van Dijk, A.I.J.M.; Levizzani, V.; Schellekens, J.; Miralles, D.G.; Martens, B.; De Roo, A. MSWEP: 3-hourly 0.25° global gridded precipitation (1979–2015) by merging gauge, satellite, and reanalysis data. *Hydrol. Earth Syst. Sci.* **2017**, *21*, 1–38. [[CrossRef](#)]
46. Condom, T.; Rau, P.; Espinoza, J.C. Correction of TRMM 3B43 monthly precipitation data over the mountainous areas of Peru during the period 1998–2007. *Hydrol. Process.* **2011**, *25*, 1924–1933. [[CrossRef](#)]
47. Brown, J.E.M. An analysis of the performance of hybrid infrared and microwave satellite precipitation algorithms over India and adjacent regions. *Remote Sens. Environ.* **2006**, *101*, 63–81. [[CrossRef](#)]
48. Su, F.G.; Gao, H.L.; Huffman, G.J.; Lettenmaier, D.P. Potential utility of the real-time TMPA-RT precipitation estimates in streamflow prediction. *J. Hydrometeorol.* **2011**, *12*, 444–455. [[CrossRef](#)]
49. Su, F.G.; Hong, Y.; Lettenmaier, D.P. Evaluation of TRMM Multisatellite Precipitation Analysis (TMPA) and its utility in hydrologic prediction in the La Plata Basin. *J. Hydrometeorol.* **2008**, *9*, 622–640. [[CrossRef](#)]
50. Wilks, D.S. *Statistical Methods in the Atmospheric Sciences: An Introduction*; Academic Press: New York, NY, USA, 1995.
51. Shen, Y.; Hong, Z.; Pan, Y.; Yu, J.J.; Maguire, L. China’s 1 km Merged Gauge, Radar and Satellite Experimental Precipitation Dataset. *Remote Sens.* **2018**, *10*, 264. [[CrossRef](#)]
52. Xu, Z.X.; Zhang, N. Long-term trend of precipitation in the Yellow River basin during the past 50 years. *Geogr. Res.* **2006**, *25*, 27–34. (In Chinese)
53. Ke, S.J.; Wang, L. Analysis of the Precipitation Law in the Yellow River Basin. *Yellow River* **1997**, *7*, 18–22. (In Chinese)
54. Knapp, K.R. Scientific data stewardship of international satellite cloud climatology project B1 global geostationary observations. *J. Appl. Remote Sens.* **2008**, *2*, 142–154. [[CrossRef](#)]
55. Sorooshian, S.; Hsu, K.L.; Ashouri, H.; Braithwaite, D.; Nguyen, P.; Thorstensen, A.R. PERSIANN-CDR Daily Precipitation Dataset for Hydrologic Applications and Climate Studies. In Proceedings of the AGU Fall Meeting, San Francisco, CA, USA, 14–18 December 2015.
56. Joyce, R.J.; Xie, P.P. Kalman Filter-Based CMORPH. *J. Hydrometeorol.* **2011**, *12*, 1547–1563. [[CrossRef](#)]
57. Mccollum, J.R.; Krajewski, W.F.; Ferraro, R.R.; Ba, M.B. Evaluation of Biases of Satellite Rainfall Estimation Algorithms over the Continental United States. *J. Appl. Meteorol.* **2002**, *41*, 1065–1080. [[CrossRef](#)]
58. Liu, J.; Shangguan, D.; Liu, S.Y.; Ding, Y.J.; Wang, S.P.; Wang, X.N. Evaluation and comparison of CHIRPS and MSWEP daily-precipitation products in the Qinghai-Tibet Plateau during the period of 1981–2015. *Atmos. Res.* **2019**, *230*, 104634. [[CrossRef](#)]
59. Liu, J.F.; Chen, R.S.; Han, C.T.; Tan, C.P. Evaluating TRMM multi-satellite precipitation analysis using gauge precipitation and MODIS snow-cover products. *Adv. Water Sci.* **2010**, *21*, 343–348. (In Chinese)
60. Wang, S.X.; Zhang, L.P.; Yu, X.Y.; She, D.X.; Gan, Y.Y. Application of Remote Sensing Precipitation Products in Runoff Simulation over the Lancang River Basin. *Resour. Environ. Yangtze Basin* **2019**, *28*, 1365–1374. (In Chinese)
61. Deng, X.X.; Ye, A.Z.; Mao, Y.; Lang, Y.; Xu, J. TRMM Precipitation Evaluation for Inland of China. *J. China Hydrol.* **2015**, *35*, 47–54. (In Chinese)
62. Luo, S.; Miao, J.F.; Niu, T.; Wei, C.X.; Wang, X. A Comparison of TRMM 3B42 Products with Rain Gauge Observations in China. *Meteorol. Mon.* **2011**, *37*, 1081–1090. (In Chinese)

63. Hu, Q.F.; Yang, D.W.; Wang, Y.; Yang, H.B. Accuracy and spatio-temporal variation of high resolution satellite rainfall estimate over the Ganjiang River Basin. *Sci. China* **2013**, *56*, 853–865. [[CrossRef](#)]
64. Cheng, K.Y.; Zhang, L.L.; Kang, Y.; Zhang, J.Y.; Liu, G.B.; Shen, X.Q. Applicability Analysis of Various Satellite-based Precipitation in Oujiang Basin. *Water Resour. Power* **2016**, *34*, 15–19. (In Chinese)
65. Li, R.Z.; Zhang, A.D.; Zhang, H.; Jiang, D.J. Accuracy evaluation of multi-satellite precipitation products over Circum-Bohai-Sea Region. *Chin. J. Appl. Ecol.* **2016**, *27*, 2916–2924. (In Chinese)
66. Wei, L.Y.; Jiang, S.H.; Ren, L.L.; Zhang, L.Q.; Zhou, M.Y. Evaluation and Comparison of Multi-Source Satellite Precipitation Products in Different Climate Regions over Mainland China. *China Rural Water Hydropower* **2019**, *0*, 38–44. (In Chinese)
67. Wang, Y.D.; Chen, H.; Liu, C.R.; Ding, Y.J. Applicability of ITPCAS and CMORPH Precipitation Datasets over Shaanxi Province. *Arid Zone Res.* **2018**, *35*, 579–588. (In Chinese)
68. Xu, S.G.; Niu, Z.; Shen, Y.; Da, K. A Research into the Characters of CMORPH Remote Sensing Precipitation Error in China. *Remote Sens. Technol. Appl.* **2014**, *29*, 189–194. (In Chinese)
69. Xu, S.G.; Niu, Z.; Shen, Y.; Kuang, D. Evaluation and Modification of CMORPH Multi-satellite Precipitation Estimates in Summer over Tibetan Plateau. *Remote Sens. Inf.* **2015**, *30*, 71–76. (In Chinese)
70. Jin, X.L.; Shao, H.; Zhang, C.; Yan, Y. The Applicability Evaluation of Three Satellite Products in Tianshan Mountains. *J. Nat. Resour.* **2016**, *31*, 2074–2085. (In Chinese)
71. Gao, Y.; Xu, H.; Guo, L. Evaluation of the GSMaP Estimates on Monitoring Extreme Precipitation Events. *Remote Sens. Technol. Appl.* **2019**, *34*, 1121–1132.
72. Zeng, S.K.; Yong, B. Evaluation of the GPM-based IMERG and GSMaP precipitation estimates over the Sichuan region. *Acta Geogr. Sin.* **2019**, *74*, 1305–1318. (In Chinese)
73. Fu, Q.N.; Ruan, R.Z.; Liu, Y.B. Accuracy Assessment of Global Satellite Mapping of Precipitation (GSMaP) Product over Poyang Lake Basin, China. *Procedia Environ. Sci.* **2011**, *10*, 2265–2271. [[CrossRef](#)]
74. Zhou, X.; Ni, G.H.; Zhong, Z.Y.; Guo, S. Evaluation of Accuracy and Streamflow Simulation of TRMM Satellite Precipitation Data. *J. Water Resour. Res.* **2019**, *8*, 125–135. (In Chinese) [[CrossRef](#)]
75. Siddique-E-Akbor, A.H.M.; Hossain, F.; Sikder, S. Satellite Precipitation Data-Driven Hydrological Modeling for Water Resources Management in the Ganges, Brahmaputra, and Meghna Basins. *Earth Interact.* **2014**, *18*, 1–25. [[CrossRef](#)]
76. Tam, T.H.; Rahman, A.M.Z. Application of Satellite Rainfall Products for Flood Inundation Modelling in Kelantan River Basin, Malaysia. *Hydrology* **2019**, *6*, 95. [[CrossRef](#)]
77. Mazzoleni, M.; Bhattacharya, B.; Barajas, M.A.L. Exploring the use of the three rainfall remote sensing products for flood prediction in the Brahmaputra basin. *EPiC Ser. Eng.* **2018**, *3*, 1366–1372.
78. Fallah, A.; Orth, R. Climate-dependent propagation of precipitation uncertainty into the water cycle. *Hydrol. Earth Syst. Sci.* **2020**. discussed manuscript.
79. López, P.L.; Sutanudjaja, E.H.; Schellekens, J.; Sterk, G.; Bierkens, M.F. Calibration of a large-scale hydrological model using satellite-based soil moisture and evapotranspiration products. *Hydrol. Earth Syst. Sci.* **2017**, *21*, 3125–3144. [[CrossRef](#)]
80. Shrestha, A.; Nair, A.S.; Indu, J. Role of precipitation forcing on the uncertainty of land surface model simulated soil moisture estimates. *J. Hydrol.* **2020**, *580*, 124264. [[CrossRef](#)]
81. Xu, Z.; Wu, Z.; He, H. Evaluating the accuracy of MSWEP V2. 1 and its performance for drought monitoring over mainland China. *Atmos. Res.* **2019**, *226*, 17–31. [[CrossRef](#)]

